Title

CROSS SECTION AND VECTOR ANALYZING POWER iT11 OF THE PROCESSES 3He(d,d)3He(d,p)4He BETWEEN 15 AND 40 MeV

Author

Roy, R.

Publication Date

1981-12-01

LBL-14343
Preprint

Lawrence Berkeley Laboratory
UNIVERSITY OF CALIFORNIA

Published in Physical Review C, Vol. 24, No. 6,
December 1981, pp. 2421-2434.

CROSS SECTION AND VECTOR ANALYZING POWER iT_{11} OF THE PROCESSES $^3He(\vec{d},d)^3He(\vec{d},p)^4He$ BETWEEN 15 and 40 MeV

R. Roy, F. Seiler, H.E. Conzett, and F.N. Rad

December 1981

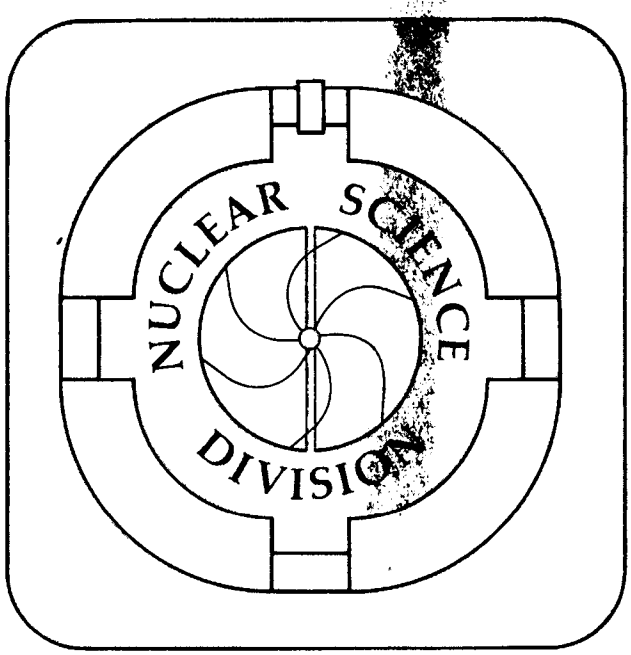

Prepared for the U.S. Department of Energy under Contract DE-AC03-76SF00098

DISCLAIMER

Cross Section and Vector Analyzing Power iT_{11} of the Processes $^3He(\vec{d},d)^3He$ and $^3He(\vec{d},p)^4He$ between 15 and 40 MeV

R. Roy[†]
Lawrence Berkeley Laboratory
University of California
Berkeley, California 94720.

and

Laboratoire de Physique Nucléaire
Université Laval
Québec, Canada, G1K 7P4.

F. Seiler[Γ], H.E. Conzett and F.N. Rad[∫]
Lawrence Berkeley Laboratory
University of California
Berkeley, California 94720.

[†] Present address: Laboratoire de Physique Nucléaire, Université Laval, Québec, Canada, G1K 7P4.

[Γ] On leave of absence from the University of Basel, Basel, Switzerland.

[∫] Present address: Laboratory for Nuclear Science, MIT, Cambridge, Mass., USA.

This work was supported by the Director, Office of Energy Research, Office of Basic Energy Sciences, Nuclear Sciences Division of the U.S. Department of Energy under Contract No. DE-AC03-76SF00098.

E

NUCLEAR REACTIONS $^3He(\vec{d},d)^3He$, $^3He(\vec{d},p)^4He$, E_d = 14.6 to 39.9 MeV measured vector analyzing power $iT_{11}(E_d,\theta)$ and cross section $\sigma_o(E_d,\theta)$. Optical model and DWBA analysis.

ABSTRACT

Differential cross-sections $\sigma_o(\theta)$ and angular distributions of the vector analyzing power $iT_{11}(\theta)$ have been measured for the processes $^3He(\vec{d},d)^3He$ and $^3He(\vec{d},p)^4He$ from 15 to 40 MeV in intervalls of 5 MeV. Data were obtained typically at 25 to 35 angles. In both reactions the angular distributions of the observables, expanded in terms of Legendre polynomials, clearly show structure near 20 and 35 MeV. In addition an optical model fit to the elastic scattering data was made and used in an attempt at a DWBA analysis of the reaction data.

I INTRODUCTION

The mass-5 system has been the object of numerous experimental and theoretical studies in the past several years[1,2,3]. The availability of polarized deuteron beams and polarized ^{3}He-targets allowed a detailed experimental study of the systems $\vec{d}+^3H$ (refs. 4-5) and $\vec{d}+^3He$ (refs. 6,7) as well as $d+^3\vec{He}$ (refs. 8-10) and $\vec{d}+^3\vec{He}$ (ref. 11). Measurements of the polarization of the outgoing nucleon[12-15] and polarization transfer experiments $^3H(\vec{d},\vec{n})^4He$ and $^3He(\vec{d},\vec{p})^4He$ have also been carried out at several energies[5,16-19]. Recently sources of polarized tritons and ^{3}He particles have become operational, considerably broadening the range of investigations[20-22]. With measurements of all these observables avalaible, complete experiments are a distinct possibility[23,24]. In addition precise phase-shift analyses of nucleon-^{4}He elastic scattering[25,26] up to 55 MeV and a variety of other nuclear reactions have provided detailed information on the intermediate system over a wide range of excitation energies[3]. On the theoretical side microscopic calculations, using a cluster approach, have been very successful in providing new insights into the structure of the five-nucleon system and the processes in which it is formed[27-31].

The $^3He(d,p)^4He$ reaction is a particularly suitable process for both theoretical and experimental investigations. Its spin structure is already quite complex, but polarized beams or targets can be prepared for all reactants with spin, making a large number of observables available for a detailed comparison of theory and experiment. The present work extends the range of vector polarization studies of the processes $^3He(\vec{d},d)^3He$ and $^3He(\vec{d},p)^4He$ from 15 to 40 MeV in 5 MeV intervalls. Complete differential cross-sections $\sigma_0(\theta)$ and angular distributions of the vector analyzing power $iT_{11}(\theta)$ have been measured at all energies. Cross-sections and angular-distributions of polarization for both processes were analyzed in terms of Legendre polynomials. The resulting coefficients were investigated for energy-dependent features such as those predicted by some analyses and models[27,30-32]. In addition, the elastic scattering data were fitted with an optical model code, while the reaction data were parametrized by DWBA calculations.

II EXPERIMENTAL ARRANGEMENT

A purely vector polarized beam of the Berkeley 88" cyclotron impinged on a ^{3}He gas target in a 36" scattering chamber. The beam polarization was monitored in a $^4He(\vec{d},d)^4He$ polarimeter located further downstream. Typically about 80% of the maximum possible value ($P_y = 2/3$) was found, using a calibration published earlier[33]. During a run the polarization usually remained constant to withing 0.01.

The detection system consisted of three detector arrangements mounted 10^o apart on each side of the beam. At the most forward angle an E - ΔE telescope allowed the simultaneous identification of ^{3}He and ^{4}He recoils from the $^3He(d,d)^3He$ and $^3He(d,p)^4He$ processes, respectively. The second system consisted of two detectors to measure the deuteron and proton spectra separately, using appropriate aluminum absorbers to separated deuterons from ^{3}He particles. The third system was a single detector with an absorber thick enough to stop all reaction partners except protons. Two fixed detectors, set a $\theta = 22^o$ and placed at $\pm 7^o$ with respect to the normal on the scattering plane, provided a relative normalization between individual runs. At each energy a run with an unpolarized beam provided an absolute measurement of the cross-sections and thus allowed a calibration of the monitors.

The peaks in the spectra at the lower energies were usually very well separated, allowing straightforward summation over the peaks. Background subtraction was needed with increasing energy, predominantly at forward angles. Deadtime corrections were applied, amounting to several percent for some of the forward angle data. The systematic errors of the cross-sections for both processes are estimated to be less than 10%.

III RESULTS

The present data for elastic scattering are in satisfactory agreement with measurements of cross-sections and vector-analyzing power[34,35] at lower energies (figs. 1 and 2). At comparable energies the cross-sections agree well with available data[35-37] except at 39.2 MeV[36] where there is a discrepancy in the dip near c.m. angles of 100-110 degrees.

The cross-sections of the $^3He(d,p)^4He$ reaction presented here are systematically lower than those of King and Smythe[35] and those derived from measurements of the inverse reaction at 35 MeV[38-40]. However, there is good agreement with other cross-section values at 25 MeV[37] and both observables join smoothly to values at lower energies (figs. 3 and 4) measured by the Zürich group[41].

The present data, summarized in figs. 5 and 6, show few and only gradual changes in the angular distributions of both observables. The vector analyzing power reaches relatively large fractions of the maximum possible valeus ($iT_{11} = \pm\frac{1}{2}\sqrt{3}$), mostly at rear angles for elastic scattering but at forward angles for the proton reaction. In the latter the angular distribution of iT_{11}, which is essentially antisymmetric with regard to 90^o at 11.5 MeV and below (refs. 7, 41 and fig. 4), changes to a more symmetric appearance between 20 and 30 MeV. The elastic scattering data on the other hand show little change over the entire energy region.

IV ANALYSIS

A. Discussion of the Legendre polynomial fits

Both the cross-sections $\sigma_o(\theta)$ and the quantities $C_{11}(\theta) = -2iT_{11}(\theta) \cdot \sigma_o(\theta)$, derived from the vector analyzing power, were parametrized by expansions in terms of appropriate Legendre polynomials. The normalized expansion coefficients $d_{00}(L)$ and $d_{11}(L)$, are then given by[30]

$$\frac{4\pi}{\sigma_{tot}} \cdot \sigma_o(\theta) = \sum_L d_{oo}(L) P_L(\cos\theta$$

$$\frac{4\pi}{\sigma_{tot}} \cdot \sigma_o(\theta) \{-2iT_{11}(\theta)\} = \sum_L d_{11}(L) P_{L,1}(\cos\theta).$$

The maximum degree L_m of the polynomials used was determined in the usual manner, except in cases where a generally nonzero coefficient crosses zero as a function of energy. In these circumstances that particular coefficient was also allowed to vary freely. The values of maximum degree L_m, determined in this manner, varied between 8 and 12. With 25 to 35 data points per angular distribution, the resulting degrees of freedom of the fits were sufficiently large for a reliable determination of the coefficients. In figs. 7 and 8 they are given for $^3He(d,d)^3He$ elastic scattering and in figs. 9 and 10 for the $^3He(d,p)^4He$ reaction. The resulting fits are shown as the solid lines in figs. 5 and 6, while the total cross-sections derived from the analysis are given in fig. 11 and table 1. The values of the coefficients for the $^3He(d,p)^4He$ reaction below 11.5 MeV were taken from the work of the Zürich group[7]. Mostly, they establish a trend leading directly to the values presented here.

The cross-section $\sigma_o(\theta)$ for elastic scattering of the deuterons shows a strong energy-dependent structure of the coefficients $d_{00}(L)$ near 35 MeV and a weaker one near 20 MeV (fig.7). While almost all coefficients

are strongly affected at the higher energy, the structure near 20 MeV shows best in the coefficients of higher degree L. A similar situation obtains for the cross-section of the $^3He(d,p)^4He$ reaction (fig.9). The structure at higher energies, however, is not nearly as dominant, while the one at the lower energy affects again all coefficients.

The expansion coefficients $d_{11}(L)$ show quite generally less structure. In elastic scattering (fig. 8) they are small and do not vary strongly with energy, although they show perturbations near both 20 and 35 MeV. In the $^3He(\vec{d},p)^4He$ reaction, almost no corresponding structure can be discerned at 35 MeV, while the one at 20 MeV is very weak (fig. 10). In this process, however, the main energy dependent features are shown by coefficients $d_{11}(1)$ and $d_{11}(2)$. At low energies the $L = 2$ term is large and dominates all others. As the energy increases toward 20 MeV, it goes to small values, while the initially unimportant $L = 1$ coefficient becomes large enough to determine the gross structure of the angular distribution.

This change can be interpreted in terms of intermediate states in the ^5Li system[3,30,31]. An expansion coefficient $d_{kq}(L)$ is a linear combination of a set of interference terms $R_1R_2^*$ of reaction amplitudes $R_i \equiv \langle \ell_i', s_i', J_i^\pi | R | \ell_i, s_i, J_i^\pi \rangle$. A restriction required by parity conservation for all first order and some second order polarization observables[30] is that the interference term must satisfy the condition $\ell_1+\ell_2+L$ = even. Therefore the L = even terms involve combinations of reaction matrix elements with equal parity, while opposite parities lead to contributions to the L = odd coefficients. The predominance of the coefficients $d_{11}(2)$ thus supports the result of calculations by Heiss and Hackenbroich[27] which lead to strong interference terms between members of a quartet of d-wave resonances. Further experimental evidence is supplied by two recent analyses of the reaction [30,31]. Correspondingly, the rise in importance of the L = 1 coefficient with increasing energy is due to terms involving matrix elements of opposite parity, such as the d-wave amplitudes and large f-wave $7/2^-$-state proposed at deuteron energies above 11.5 MeV. A further preliminary analysis along such lines[30] must await the measurement of the analyzing power for deuteron tensor polarization.

B. Optical model fit of $^3He(\vec{d},d)^3He$

It has been pointed out recently[43] that the similarity of deuteron scattering from ^3He and ^4He above $E_d \sim 8$ MeV points to a predominance of potential scattering and indicates only a weak dependence of the interaction on the spin of the target. Good optical model fits have been obtained between 10 and 14 MeV, using a very small tensor interaction, a spin-orbit term and a surface absorption[43]. Consequently, the standard optical model potential was used here in the form

$$V_{om}(r) = V_c(r_c) - V_f(r_v,a_v) -$$

$$- iW\, f(r_a,a_a) +$$

$$+ 4iW_D a_W \frac{d}{dr} f(r_W,a_W) +$$

$$+ \left(\frac{h}{m_\pi c}\right)^2 (V_{so}+iW_{so}) \frac{1}{r} \frac{d}{dr} f(r_{so},a_{so}) \vec{\ell}.\vec{s}$$

with

$$f(r_i,a_i) = \{1+\exp \frac{1}{a_i} (r-r_i A^{1/3})\}^{-1} .$$

The optical model fits were obtained by using the code MAGALI[44].

Starting values for the analyses were obtained by an inspection of previous analyses of deuteron scattering from light nuclei[43,45]. During the initial runs it became apparent, that both absorption terms W and W_{so} could indeed be set to zero without appreciably affecting the fits. Also automatic searches were only successful if the surface diffuseness parameters a_W and a_{so} were kept constant until a fit was nearly obtained. Since average optimum values of $a_W = 0.35$ fm and $a_{so} = 0.30$ fm were found in grid searches troughout the energy range, they were always kept constant. This procedure resulted in the parameter set A of table 2. The resulting fits are given in figs. 12 and 13 (solid lines). In order to get fits somewhat closer to the data at 35 and 40 MeV, it was

necessary to use values for r_w quite different from the optimum average found for the lower energies. All other geometric parameters were kept the same at all energies; even so, the potential strengths W_d and V_{so} vary strongly with energy. A search on more free parameters would give a better fit at each energy but the parameters a and r would be fairly different from one set of data to another. For each set of parameters of table 2, the values were first varied to obtain the best fit for the 14.6 MeV data. Then those values became the starting values at the next higher energy. The procedure was subsequently repeated throughout the energy range.

Starting values more like the parameters obtained from another lower-energy analysis[40] led to set B of table 2. In this case it was attempted to keep all diffuseness values more or less the same instead of the radius values (set A). Again, some parameters changed considerably above 30 MeV. However,the potential strengths changed in a less drastic way, when some geometric parameters were allowed to deviate strongly from their values at lower energy. Figs. 12 and 13 show those fits as dashed lines. For the data up to 30 MeV, two other calculated curves are presented. The set C leads to fits in general quite different from those originating from sets A and B. The set D, found by searching on radius values and potential strngths of set C is not very different, and the radii exhibit a variation with energy which is to be expected.

The three first sets of table 2 represent distinct families based on different values of the product[46] $V.(r_v)^n$ with $n \simeq 2$. The resulting fits display various features for each group of parameters, as can be seen in figs. 12 and 13.

C. DWBA analysis of the $^3He(d,p)^4He$ reaction

In the past, several analyses have been carried out on the $^3He(d,p)^4He$ reaction. Diffraction and PWBA theories have been used at different energies[37-39,47] around E_p = 47 MeV in the laboratory, but sophisticated PWBA theories were not appreciably more successful in representing the angular distributions[47]. The need of a lower cut-off in the radial overlap integrals to achieve reasonably good agreement was a common conclusion drawn from investigations with PWBA theory[38,47]. A sensitivity to the lower cut-off radius was observed in the case of the DWBA approach[37-47]. A fairly good DWBA representation has been obtained[38] without a cut-off radius, but it was pointed out by the authors that the interpretation of the opticam model parameters was ambiguous for both incident and exit channels.

In the present calculations, the code DWBA[48] has been used to obtain cross-section and vector analyzing-power angular distributions with the optical model parameters from table 2 in the entrance channel and from an optical model analysis[49] of proton scattering on ^4He between 31 and 55 MeV. In the case of the proton channel, parameters corresponding to the closest c.m. energy have been chosen for each incident energy. Calculations in the zero range approximation (solid-lines), with a finite range correction of 1.25 fm (dashed-dotted lines) and with a cut-off radius of 3 fm (dashed lines) are presented in figs. 14 and 15. The computed curves are scaled as provied by the code, assuming a spectroscopic factor of 1.0. The different corrections applied do not change the general trend of the curves by much. The differential cross section tends in general to look more like the data at higher energy. Contrary to other calculations[47], the d-^3He optical model parameters presently used allow us to obtain computed curves the general shape of the data, although a cut-off radius is not used. This is true for the cross section data above 20 MeV (fig. 14). In fact, the data points do not show the deep minima characteristic of a cut-off radius[40,47].

On the otherhand the corresponding analyzing power calculations (fig. 15) show variations which we much too pronounced when compared to the data. The negative maximum at forward angles its well reproduced below 30 MeV, while the general shapes change around 30 MeV and a positive maximum at back angles is too large to reproduce the slight maximum found experimentally.

A finite range correction changes the computed curves very little, as shown in figs. 14 and 15. Taking into account non-local effects does not affect the calculated angular distributions appreciably. However, changing the optical model parameters in the entrance channel does affect the shape of the curves quite seriously. As it can be seen on figs. 16 and 17, calculations at 15 and 30 MeV in the zero range approximation with set A in the entrance channel (dotted lines), look very different from results with set B (solid lines). Above 20 MeV, the set A is not able to reproduce the back angle increase in the cross section . Nevertheless, set C calculations (dashed-dotted lines), obtained in the zero range approximation, exhibit little change in the general shapes of the curves. The dashed lines at 30 MeV are zero range calculations provided by set B in the deuteron channel and by the p-^{4}He parameters used by Sawada et al.[47]; they show a limited influence of the parameters in the p channel. Finally, other calculations, not shown here, were made using the parameters from Thompson et al.[49] in the p-^{4}He channel and different deuteron parameters. Whether made with finite range or non-locality corrections or not, they gave results similar to those of figs. 14 and 15 (set B, parameters of Sagle[40] in the d-^{3}He channel 1) and to those of figs. 16 and 17 (dotted lines, set A, parameters of Lyorshin et al.[43]. Thus the deuteron parameters are again clearly separated into two categories; one family with V ~ 50 MeV and one with V ~ 150-200 MeV.

V CONCLUSION

Some interesting features have been observed in the energy variations of the coefficients $d_{00}(L)$ and $d_{11}(L)$ obtained by a Legendre polynomial expansion of data on the $^3He(d,d)^3He$ and $^3He(d,p)^4He$ reactions. First, most of the coefficients show structures around 20 MeV and near 35 MeV deuteron energy with the exception of $d_{11}(L)$ of the $^3He(d,p)^4He$ reaction. Second, the coefficient $d_{11}(2)$ of the $^3He(d,p)^4He$ reaction is predominant at low energies, but with increasing energy the $L = 1$ terms becomes prevalent. This observation can be taken as a corroboration of the results of previous work[27,30,32], in which the presence of a f-wave $7/2^-$ state in the ^5Li system and the importance of the d-wave amplitudes was postulated.

Although the optical model analysis of the $^3He(d,d)^3H$ elastic scattering between 15 and 40 MeV can give only a poor picture of the data at some energies, it seems to support the results of the Legendre polynomial analysis, since the optical model parameters (table 2) show a clear tendency for rapid change around 20 - 25 MeV and particularly at 35 MeV. However, an optical model analysis would be more conclusive if performed on a complete set of data using also a tensor polarized deuteron beam. It should be noted that such measurements are also needed to reach more definite conclusions on the ^5Li system from an analysis of Legendre polynomial coefficients.

In general, the present fit to the angular distribution of the process $^3He(d,p)^4He$ in the DWBA framework leads to the same conclusions as previous analyses. So, as pointed out in one of them[47], the rise in the experimental differential cross section at back angles is reproduced by the calculated curves, even if only the single-particle pickup process is taken into account. The effect of introducing a cut-off radius is important and seems to be needed. The same holds, but to a lesser extent, with the optical model parameters provided by the $d-^3He$ elastic scattering analysis of section 4.2.

In fact, the usual way of accounting for non-local effects in DWBA calculations is not appropriate for reactions involving light nuclei[50,51]. The contribution from the interior region must be dampened more strongly by the use of a cut-off radius. As suggested by Glendenning[50], further investigations of such a reaction might provide a better agreement with the data, if they were based on the adiabatic model for the deuteron optical potential[51], a procedure already used in a few cases[51,52].

Finally, the calculations shown here allow to discriminate between the different sets of optical model parameters for the d-^{3}He channel. The set A of table 2, or parameters of the same family such as those from the work of Lyovshin et al.[43], have to be excluded on the basis of the general shape of the differential cross sections (fig. 16). In fact, this conclusion is only to be expect in view of the values of the parameters V, r_V and r_W. Usually the depth of the deuteron potential V is about twice that of the nucleon potential (~ 2 x 50 MeV) or more, while r_W is greater than r_V by about 40%.

One of us (R.R.) is grateful for financial support through a fellowship of the National Research Laboratory; and one of us (F.S.) is indebted to the Swiss National Science Foundation and the Mx Geldner Stiftung for their assistance. This work was supported by the Director, Office of Energy Research, Office of Basic Energy Sciences, Nuclear Sciences Division of the U.S. Department of Energy under Contract No. DE-AC03-76SF00098.

REFERENCES

1. Proc. 4 th Int. Symp. on Polarization Phenomena in Nuclear Reactions, W. Grüebler and V. König, eds., (Birkhäuser, Basel 1976).

2. Proc. 3rd Int. Symp. on Polarization Phenomena in Nuclear Reactions, H.H. Barschall and W. Haeberli, eds., (University of Winsconsin Press, 1971).

3. F. Ajzenberg-Selove, Nucl. Phys. A320, 1 (1979).

4. H. Grunder, R. Gleyvod, G.P. Lietz, G. Morgan, H. Rudin, F. Seiler and A. Stricker, Helv. Phys. Acta 44, 622 (1971).

5. J.W. Sunier, R.V. Poore, R.A. Hardekoptf, L. Morrison, G.C. Salzmann and G.G. Ohlsen, Phys. Rev. C 14, 8 (1976).

6. B. Jenny, W. Grüebler, V. König, P.A. Schmelzbach, R. Risler, D.O. Boersma and W.G. Weitcamp, ref. 1, p. 538.

7. W. Grüebler, V. König and P.A. Schmelzbach, Results of measurements and analyses of nuclear reactions induced by polarized and unpolarized deuterons, Eidgenossische Technische Hochschule, Zürich, internal report, May 1973.

8. U. Rohrer, P. Huber, Ch. Leemann, H. Meiner and F. Seiler, Helv. Phys. Acta 44, 899 (1971), and references therein.

9. Ch. Leemann, H. Meiner, U. Rohrer, J.X. Saladin, F. Seiler, P. Huber, W. Grüebler, V. König and P. Marmier, ref. 2, p. 548.

10. S.D. Baker, ref. 2, p. 899.

11. Ch. Leemann, H. Bïrgisser, P. Huber, H. Paetz gen. Schieck and F. Seiler, Helv. Phys. Acta 44, 141 (1971).

12. G.G. Ohlsen, R.A. Hardekopf, D.P. May, S.D. Baker and W.T. Armstrong, Nucl. Phys. A233, 1 (1974).

13. J.F. Clare, Nucl. Phys. A217, 342 (1973).

14. J.E. Brock, A. Chisholm, J.C. Duder, R. Garrett and R.E. White, ref. 1, p. 546.

15. G.S. Mutschler, W.B. Broste and J.E. Simmons, Phys. Rev. C 3, 1031 (1971).

16. F. Seiler, E. Baumgartner, W. Haeberli, P. Huber and H.R. Striebel, Helv, Phys. Acta 35, 385 (1962).

17. W.B. Broste, G.P. Lawrence, J.L. McKibben, G.G. Ohlsen and J.E. Simmons, Phys. Rev. Lett. 25, 1040 (1970).

18. P.W. Lisowski, R.L. Walter, R.A. Hardekopf and G.G. Ohlsen, ref. 1, p. 887.

19. R.A. Hardekopf, D.D. Armstrong, W. Grüebler, P.W. Keaton jr., and U. Meyer-Berkhout, Phys. Rev. C 8, 1629 (1973).

20. R.A. Hardekopf, G.G. Ohlsen, R.V. Poore and Nelson Jarmie, Phys. Rev. C 13, 2127 (1976).

21. G.G. Ohlsen, R.A. Hardelopf, R.L. Walter and P.W. Lisowski, ref. 1, p. 558.

22. N.T. Okumusoglu, C.O. Blyth, Nucl. Phys. A235, 45 (1979).

23. N. Simonius, Theory of polarization measurements I and II, unpublished reports and ref. 2, p. 401.

24. F. Seiler and E. Baumgartner, Nucl. Phys. A153, 193 (1970) and ref. 2, p. 518.

25. G.R. Plattner, A.D. Bacher and H.E. Conzett, Phys. Rev. C 5, 1158 (1972) and references therein.

26. N.E. Davison, S.A. Elbakr, A. Houdayer, A.M. Sourkes, W.T.H. von Oers and A.D. Bacher, Few Body Problem in Nuclear and Particle Physics, R.J. Slobodrian, B. Cujec and K. Ramavataram, eds., (Les Presses de l'Université Laval, Québec 1975), p. 539.

27. P. Heiss and H.H. Hackenbroich, Nucl. Phys. A162, 530 (1971).

28. H.H. Hackenbroich, ref. 1, p. 133.

29. F.S. Chwieroth, R.E. Brown, Y.C. Tang and D.R. Thompson, Phys. Rev. C 8, 938 (1973).

30. F. Seiler, Nucl. Phys. A187, 379 (1972) and A244, 236 (1975).

31. D.C. Dodder and G.M. Hale, private communication.

32. K. Ramavataram and S. Ramavataram, Nucl. Phys. A147, 293 (1970).

33. H.E. Conzett, W. Dahme, Ch. Leemann, J.A. McDonald and J.P. Meulders, ref. 1, p. 566.

34. V. König, W. Grüebler, R.E. White, P.A. Schmelzbach and P. Marmier, Nucl. Phys. A185, 263 (1972).

35. T.R. King and R. Smythe, Nucl. Phys. A183, 657 (1972).

36. R.W. Rutowski and E.E. Gross, Phys. Rev. C 12, 362 (1975).

37. O.M. Bilaniuk and R.J. Slobodrian, Nucl. Phys. 50, 585 (1964).

38. S.A. Harbison, R.J. Griffiths, N.M. Stewart, A.R. Johnston and G.T.A. Squier, Nucl. Phys. A152, 503 (1970).

39. J.G. Rogers, J.M. Cameron, M.B. Epsteing, G. Paic, P. Thomas, J.R. Richardson, J.W. Verba and P. Doherty, Nucl. Phys. A136, 433 (1969).

40. A. Sagle, private communication and to be published.

41. W. Grüebler, V. König, A. Ruh, P.A. Schmelzbach, R.E. White and P. Marmier, Nucl. Phys. A176, 631 (1970), and Grüebler et al. ref. 7.

42. W. Klinger, F. Dusch and R. Fleischmann, Nucl. Phys. A166, 253 (1971).

43. E.B. Lyovshin, O.F. Nemets and A.M. Yasnogorodsky, Phys. Lett. 52B, 392 (1974) and ref. 1, p. 542.

44. MAGALI, J. Raynal, Centre d'Etudes Nucléaires de Saclay, France, DPh-T/69-42.

45. H.F. Bingham, A.R. Zander, K.W. Kemper and N.R. Fletcher, Nucl. Phys. A173, 265 (1971).
R.C. Brown, J.A.R. Griffith, O. Karban, L. Mesko, J.M. Nelson and S. Roman, Nucl. Phys. A207, 456 (1973).

M.M. Meier and R.L. Walter, Nucl. Phys. A182, 468 (1972).

46. See for instance C.M. Perey and F.C. Perey, Phys. Rev. 132, 755 (1963).

47. T. Sawada, G. Paic, M.B. Eptstein and J.R. Rogers, Nucl. Phys. A141, 169 (1970).

48. J.M. Nelson and B.E.F. Macefield, Oxford University Nuclear Physics Lab. report 18/69 (1969), unpublished.

49. G.E. Thompson, M.B. Eptstein and T. Sawada, Nucl. Phys. A142, 571 (1970).

50. N.K. Glendenning, in Nuclear Spectroscopy and Reactions, Part D, edited by J. Cerny (Academic Press, New York, 1975). p. 319.
G.M. McAllen, W.T. Pinkston and G.R. Satchler, Particles Nuclei 1, 412 (1971).

51. R.C. Johnson and P.J.R. Soper, Phys. Rev. C 1, 976 (1970).

52. J.D. Harvey and R.C. Johnson, Phys. Rev. C 3, 636 (1971).
G.R. Satchler, Phys. Rev. C 4, 1485 (1971).

FIGURE CAPTIONS

Figure 1.

Comparison of the present cross-section data for the $^3He(d,d)^3He$ reaction at 14.6 MeV laboratory energy (Δ) with the data of König et al. (□, ref. 34) and of King and Smythe (—●—, ref. 35).

Figure 2.

Comparison of the present vector analysing power data for the $^3He(\vec{d},d)^3He$ reaction at 14.6 MeV (●) with the data of König et al. (□ ref. 34) at 11.5 MeV.

Figure 3.

Comparison of the present cross section data for the $^3He(d,p)^4He$ reaction at 14.6 MeV laboratory energy (Δ) with the data of Grüebler et al. (□, ref. 44) and King and Smythe (—●—, ref. 35).

Figure 4.

Comparison of the vector analysing power data at 14.6 MeV laboratory energy (●, present work) with the data and Grüebler et al. (ref. 41) at 11.5 MeV (□) and of Klinger et al. (ref. 42) at 13.0 MeV (x).

Figure 5a and 5b.

Angular distributions of the cross section and the vector analysing power iT_{11} for the $^3He(d,d)^3He$ reaction between 14.6 and 40 MeV laboratory energy. The squares represent the angles measured using the recoil ^3He particles. The symbol is larger than the statistical error when no error bars are shown. The solid lines are the best Legendre polynomial fits.

Figure 6a and 6b.

Differential cross-section and vector analyzing power for the $^3He(d,p)^4He$ reaction between 14.6 and 40 MeV. The recoil alpha particles where detected at angles represented by squares. The symbol is larger than the statistical error when no error bars are shown. The solid lines are the best Legendre polynomial fits.

Figures 7a and 7b.

The parameters $d_{00}(L)$ of the Legendre polynomial expansion corresponding to the fits shown in fig.5 for $^3He(d,d)^3He$ scattering. When no error bars are shown, the uncertainties of the fits are larger than the symbol. The solid lines are drawn by hand to guide the eye.

Figure 8.

The parameters $d_{11}(L)$ of the Legendre polynomial expansion corresponding to the fits shown in fig. 5 for the $^3He(\vec{d},d)^3He$ data. Uncertainties larger than the size of a symbol are shown. The solid lines are drawn by hand to guide the eye.

Figure 9a and 9b.

The parameters $d_{00}(L)$ for the $^3He(d,p)^4He$ reaction data shown in fig.6. The values of the coefficients below 12 MeV were taken from ref. 41.

Figure 10.

The parameters $d_{11}(L)$ for the $^3He(\vec{d},p)^4He$ data of fig.6. The values of the coefficients below 12 MeV were taken from ref. 41.

Figure 11.

Total cross section $\sigma_T/4\pi$ for the $^3He(d,p)^4He$ reaction from the Legendre polynomial expansion analysis. The low energy results are taken from ref. 41. The dots are larger than the uncertainties of the fits.

Figure 12.

Optical model fits of the cross section for the $^3He(d,d)^3He$ scattering data between 14.6 and 40 MeV. The solid lines correspond to fits of sets A (table 2), dashed lines to sets B, dotted and dashed-dotted lines to sets C and D respectively.

Figure 13.

Same as fig. 12, but for the vector analyzing power data iT_{11}.

Figure 14.

DWBA calculations for the $^{3}He(d,p)^{4}He$ cross sections with parameters of set B for the deuteron channel and from ref.[48] for the proton channel. The solid lines were obtained in the zero range approximation, dashed-dotted lines, with a finite range correction of 1.25 fm and dashed lines, with a cut-off radius of 3.0 fm.

Figure 15.

Same as fig. 14, but for the vector analyzing-power data iT_{11}.

Figure 16.

DWBA calculations in zero range approximation with parameters of set B (solid lines), set A (dotted lines) and set C (dashed-dotted lines); the dashed line at 30 MeV is obtained with set B (d channel) and parameters (p channel) from Sawada et al.[46].

Figure 17.

Same as fig. 16, for the vector analyzing-power data iT_{11}.

TABLE 1

Total cross section values for the $^3He(d,d)^3He$ reaction

E_d MeV	$\sigma_{TOT}/4\pi$ mb
14.62	80.4 ± 0.4
19.69	75.0 ± 0.9
24.89	66.1 ± 1.3
30.02	61.2 ± 0.8
34.92	47.3 ± 0.4
39.95	37.6 ± 0.2

TABLE 2

Potential parameters for d-^{3}He elastic scattering[†]

	E_d	V	W_d	V_{so}	r_v	r_w	r_{so}	a_v	a_w	a_{so}
Set A										
	15	52.7	2.51	0.99	1.62	1.703	1.62	0.42	0.35	0.3
	20	55.1	3.36	2.75	1.62	1.703	1.62	0.42	0.35	0.3
	25	54.7	5.68	5.38	1.62	1.703	1.62	0.42	0.35	0.3
	30	57.0	5.94	5.16	1.62	1.703	1.62	0.42	0.35	0.3
	35	33.6	4.17	3.79	1.62	3.47	1.62	0.42	0.35	0.3
	40	33.1	3.77	4.70	1.62	3.38	1.62	0.42	0.35	0.3
Set B										
	15	160.9	2.82	2.14	1.6	2.6	2.0	0.317	0.317	0.317
	20	160.3	3.46	7.79	1.6	2.6	2.0	0.317	0.317	0.317
	25	159.6	4.11	8.15	1.6	2.6	2.0	0.317	0.317	0.317
	30	169.1	3.72	8.56	1.6	2.6	2.0	0.317	0.317	0.317
	35	160.1	6.03	10.70	1.7	3.0	1.7	0.25	0.317	0.25
	40	155.5	5.15	10.07	1.7	3.0	1.7	0.25	0.317	0.25
Set C										
	15	176.0	3.49	3.25	1.4	2.4	1.8	0.5	0.317	0.317
	20	200.6	4.17	4.97	1.3	2.4	1.8	0.5	0.317	0.317
	25	203.1	5.23	4.46	1.3	2.4	1.8	0.5	0.317	0.317
	30	215.4	6.28	2.67	1.3	2.2	1.8	0.4	0.317	0.317
Set D										
	15	171.9	3.53	4.56	1.417	2.688	1.868	0.5	0.317	0.317
	20	208.0	4.04	5.12	1.265	2.399	1.820	0.5	0.317	0.317
	25	206.6	5.20	4.77	1.284	2.393	1.765	0.5	0.317	0.317
	30	238.6	6.01	2.50	1.178	2.332	1.739	0.4	0.317	0.317

[†]All energies are given in MeV and lengths in fm.

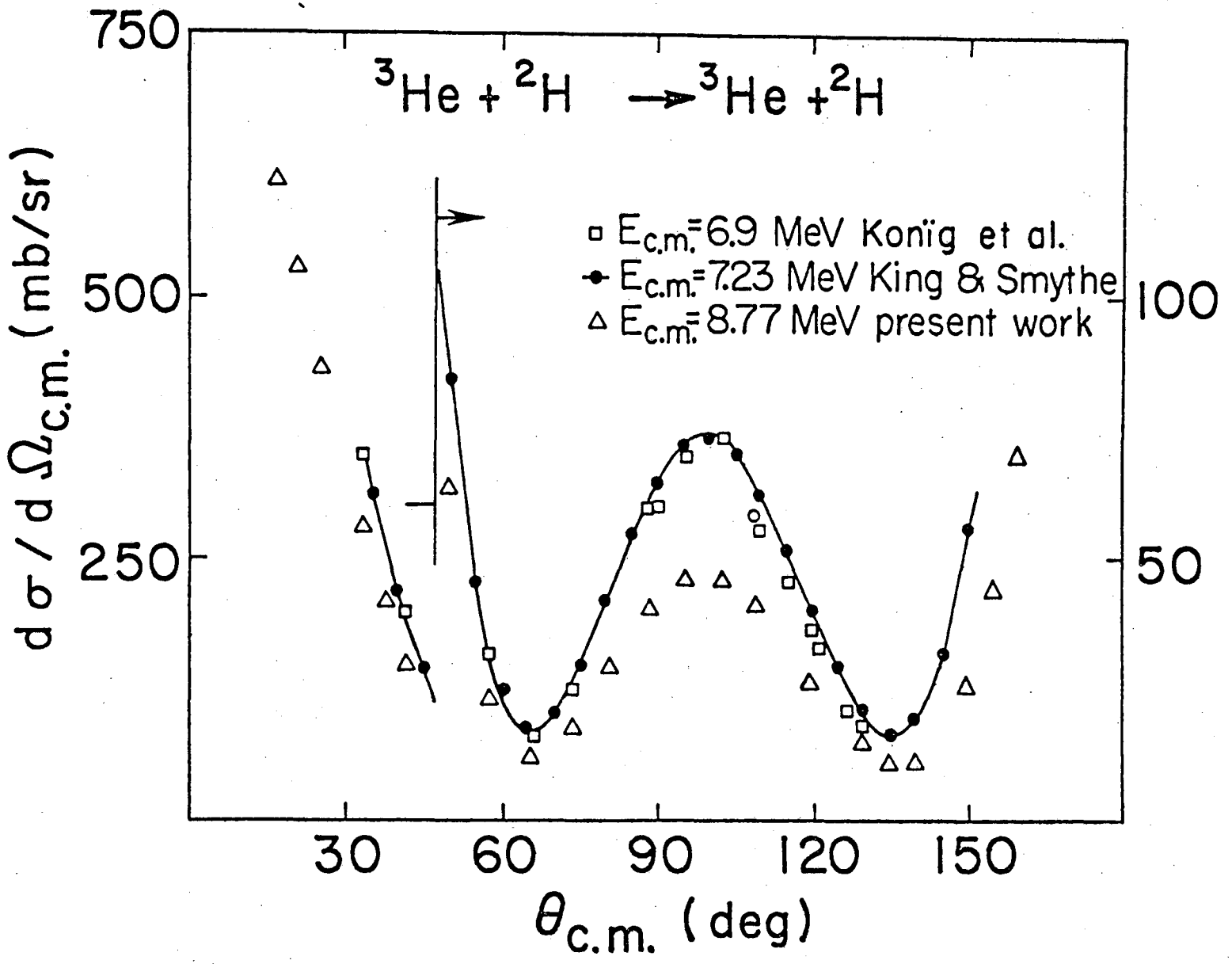

Fig. 1

XBL761-2044

LBL-14343

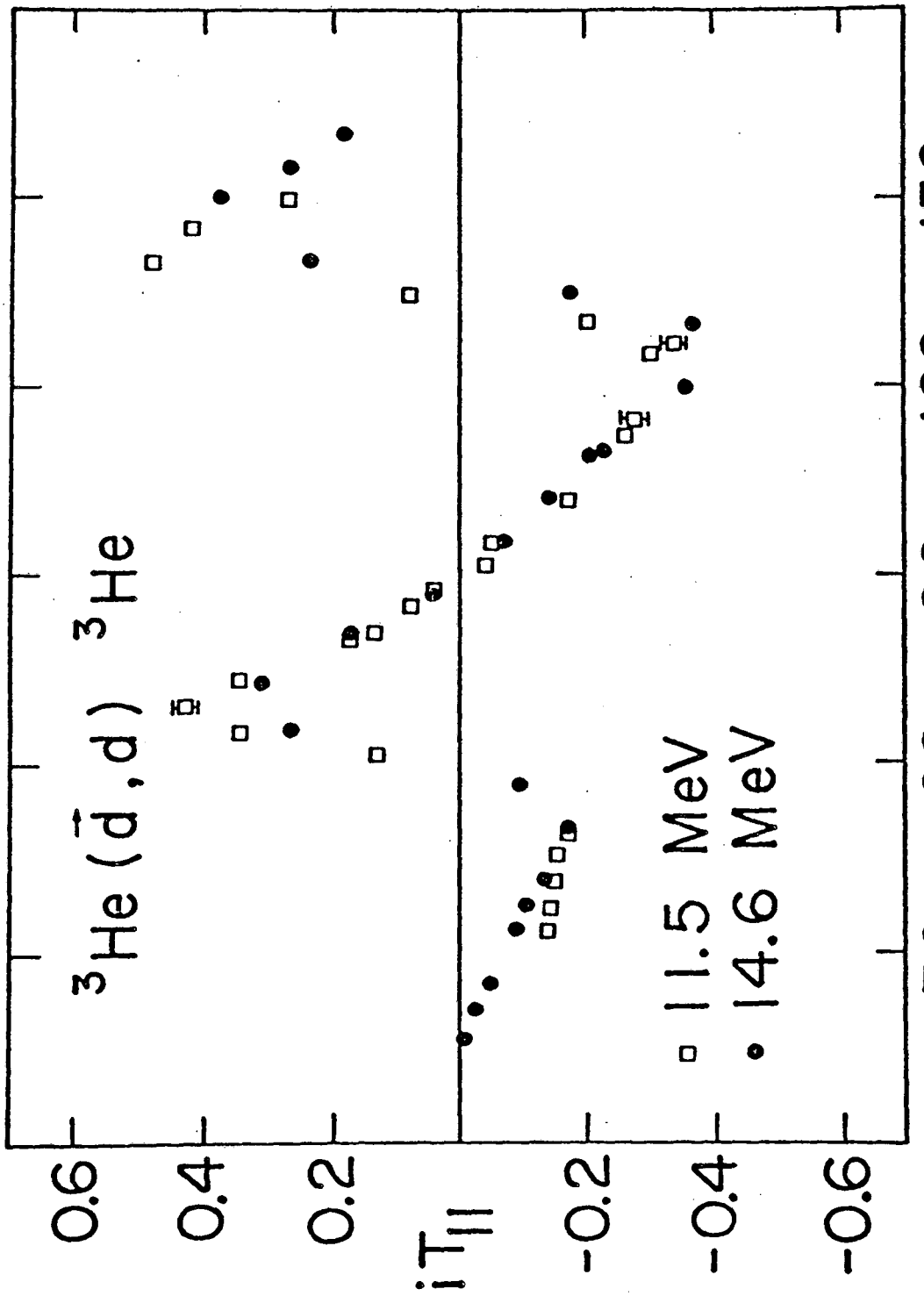

XBL761-2042

Fig. 2

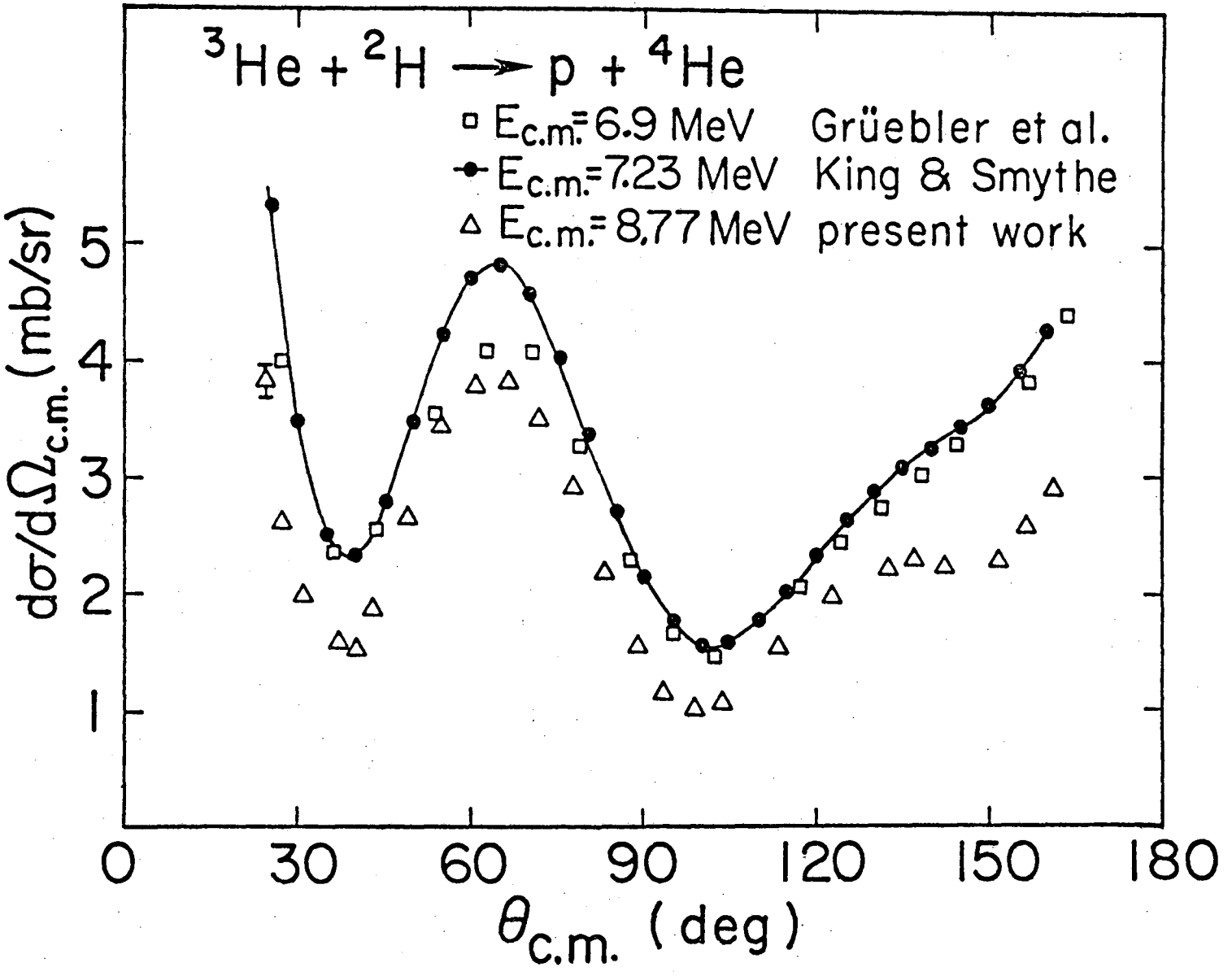

Fig. 3

XBL761-2045

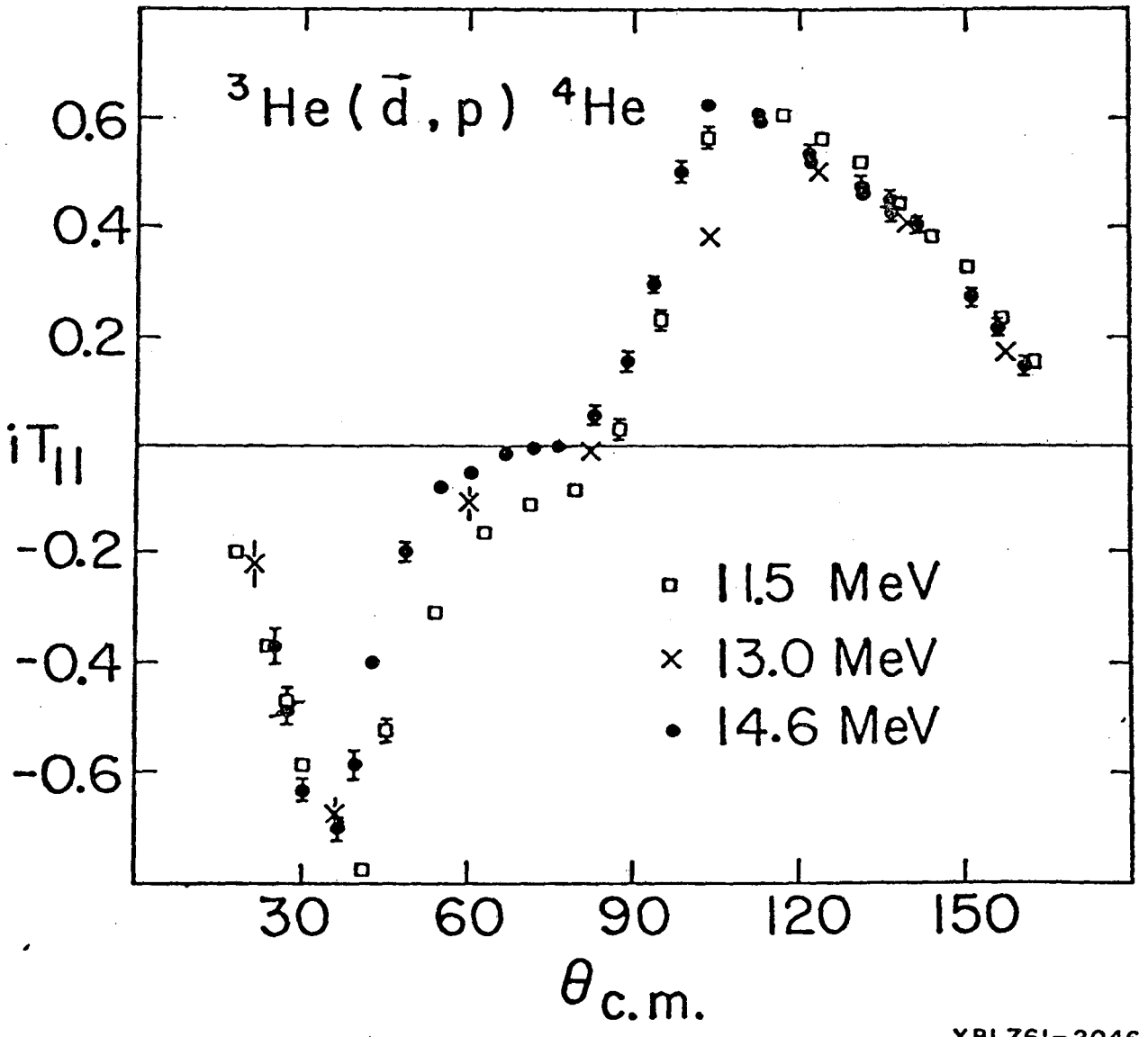

Fig. 4

XBL761-2046

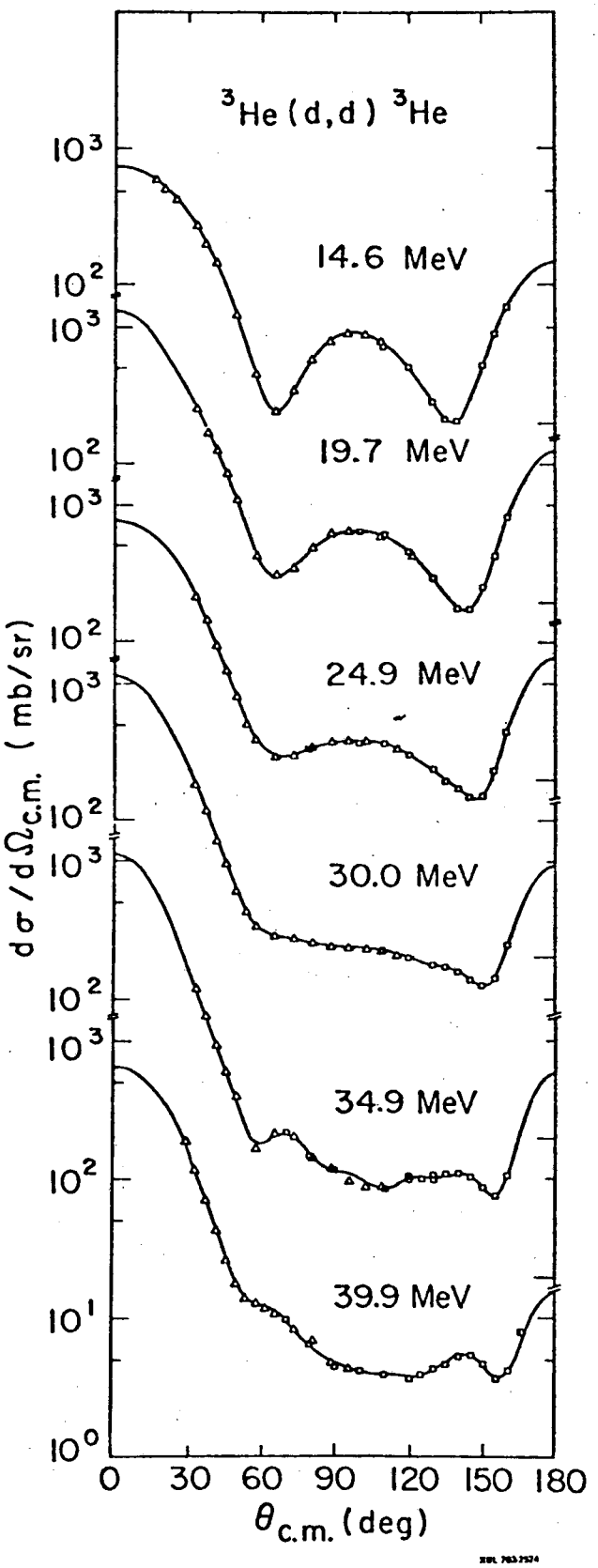
^{3}He (d,d) ^{3}He
14.6 MeV
19.7 MeV
24.9 MeV
30.0 MeV
34.9 MeV
39.9 MeV
$d\sigma/d\Omega_{c.m.}$ (mb/sr)
$\theta_{c.m.}$ (deg)
0 30 60 90 120 150 180

Fig. 5a

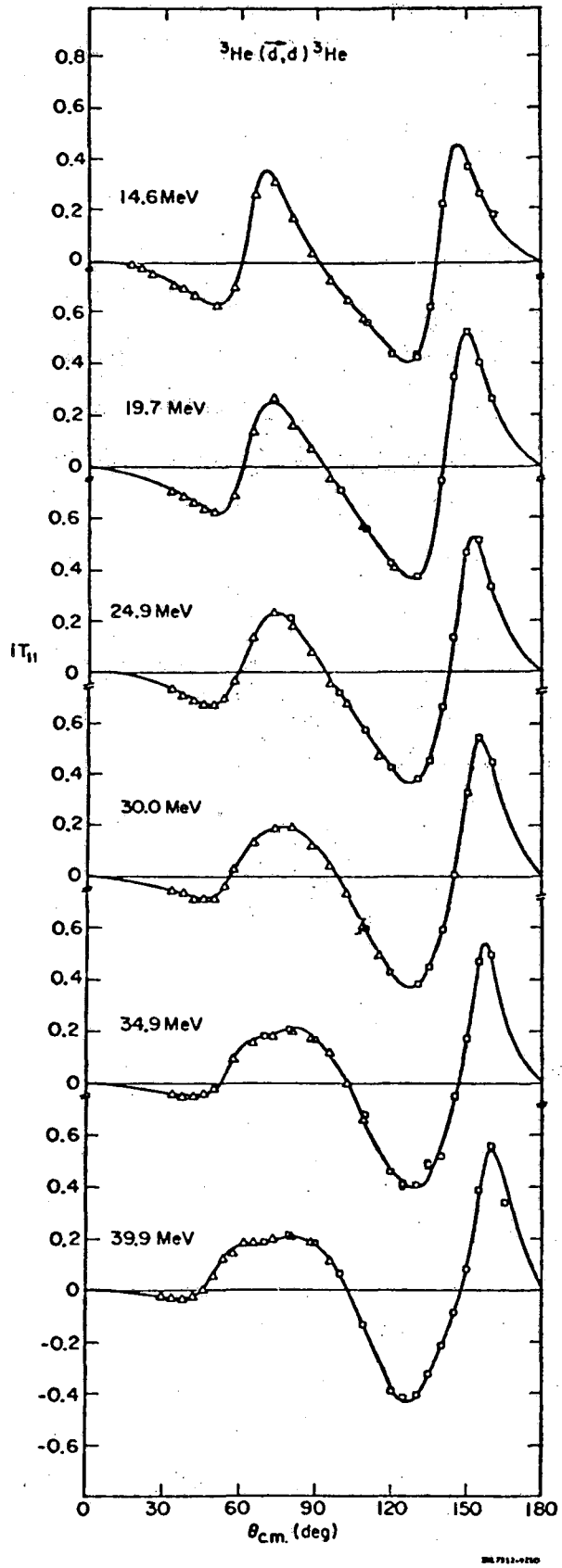
^{3}He $(\vec{d},d)^3$He
14.6MeV
19.7 MeV
24.9 MeV
30.0 MeV
34.9 MeV
39.9 MeV
iT_{11}
$\theta_{cm.}$ (deg)
0.8
0.6
0.4
0.2
0
-0.2
-0.4
-0.6
0
30
60
90
120
150
180

Fig. 5b

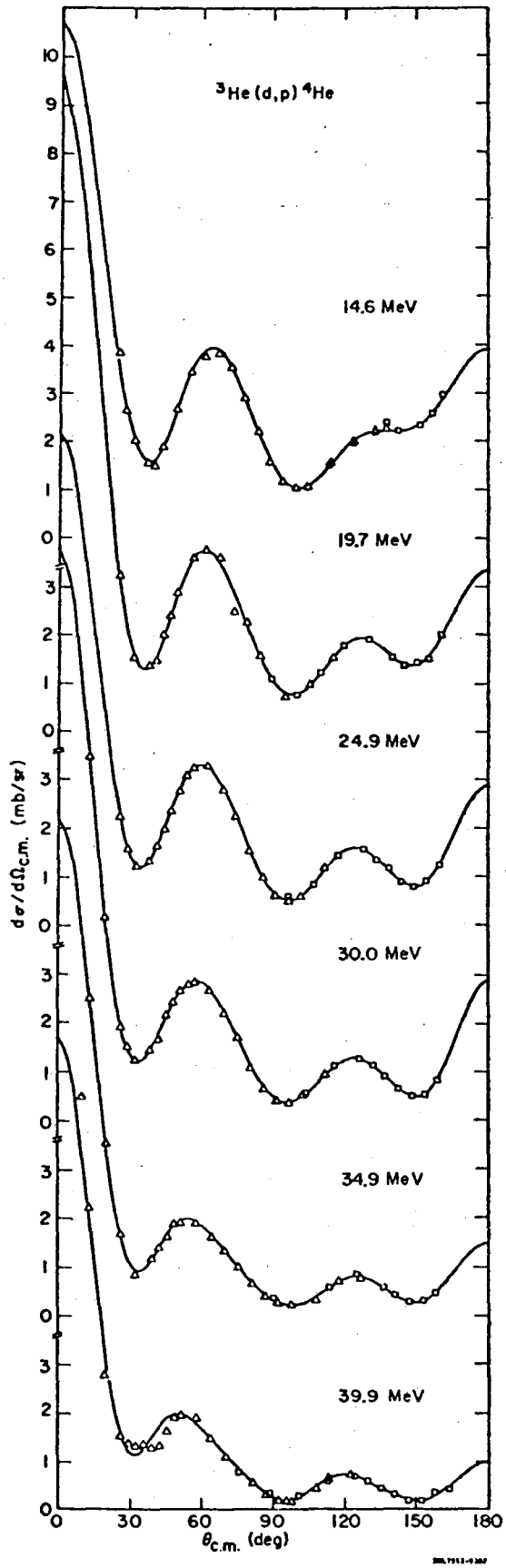
^{3}He (d,p) ^{4}He
14.6 MeV
19.7 MeV
24.9 MeV
30.0 MeV
34.9 MeV
39.9 MeV
dσ/dΩc.m. (mb/sr)
θc.m. (deg)
0
30
60
90
120
150
180

Fig. 6a

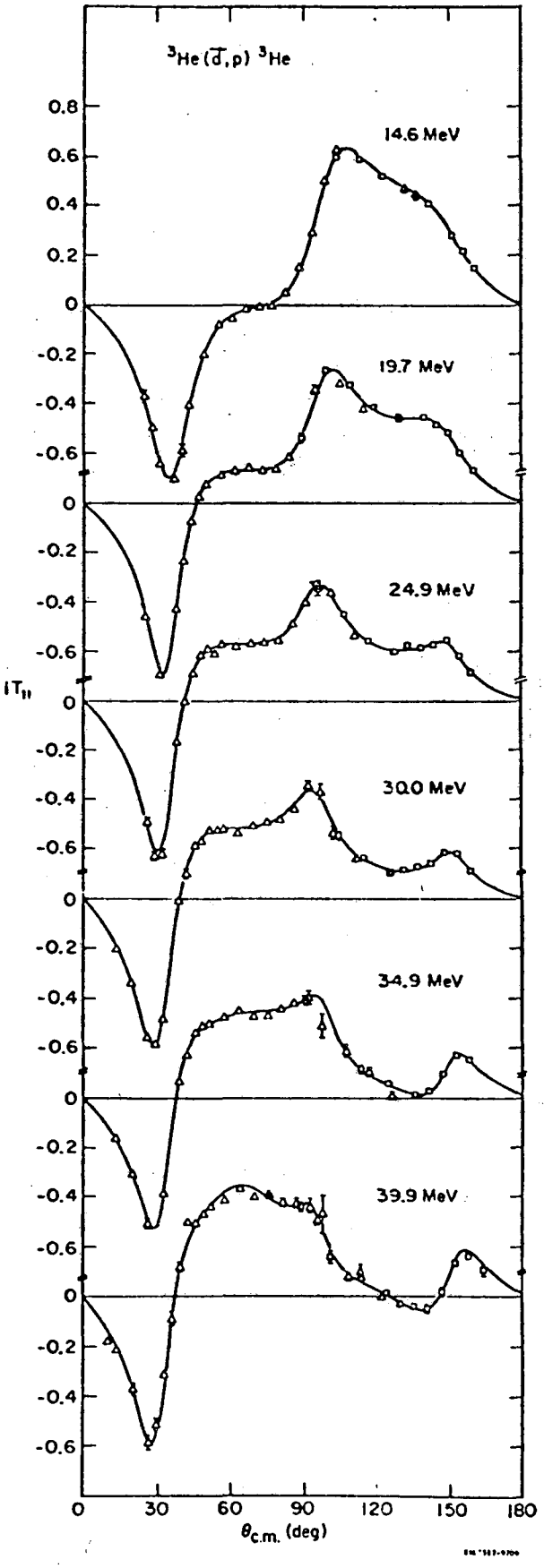
$^3He(\vec{d},p)\,^3He$
14.6 MeV
19.7 MeV
24.9 MeV
30.0 MeV
34.9 MeV
39.9 MeV
iT_{11}
$\theta_{c.m.}$ (deg)
0.8
0.6
0.4
0.2
0
-0.2
-0.4
-0.6
0
30
60
90
120
150
180

Fig. 6b

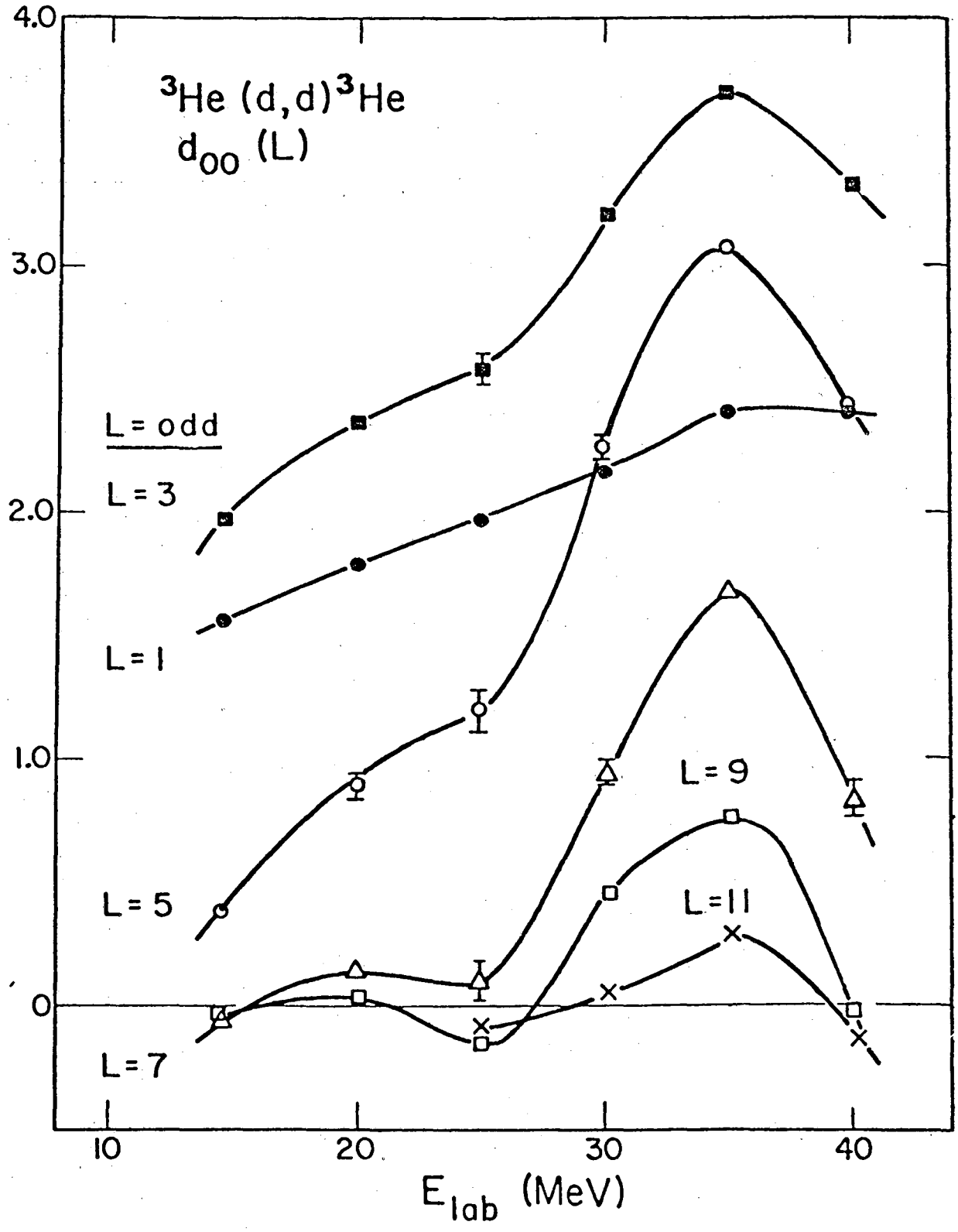

Fig. 7a

XBL 756-3190

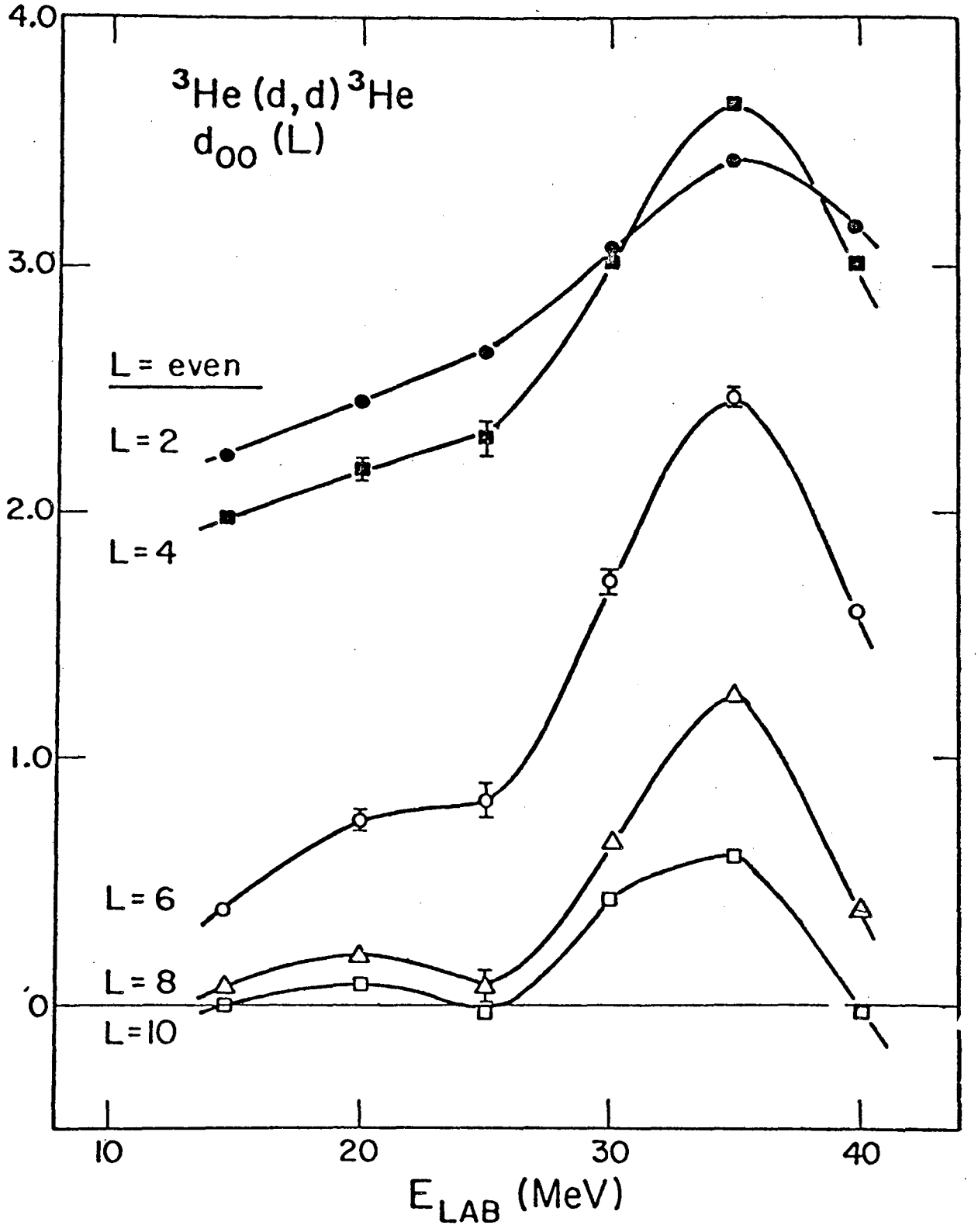

Fig. 7b

XBL 763-2521

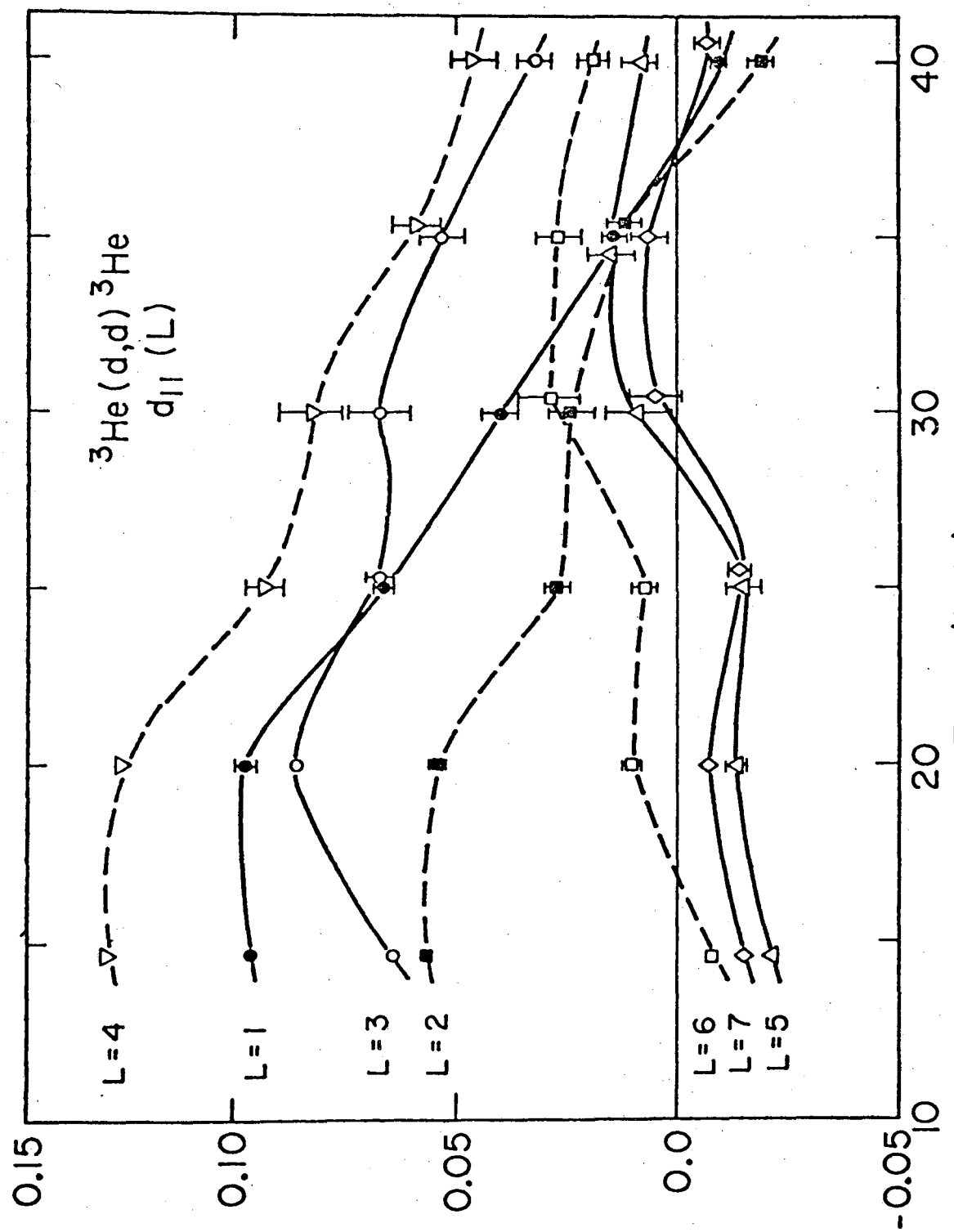
$^3He(d,d)^3He$
d_{11} (L)
L=4
L=1
L=3
L=2
L=6
L=7
L=5
0.15
0.10
0.05
0.0
-0.05
10
20
30
40
E_{lab} (MeV)
XBL 763-2520

Fig. 8

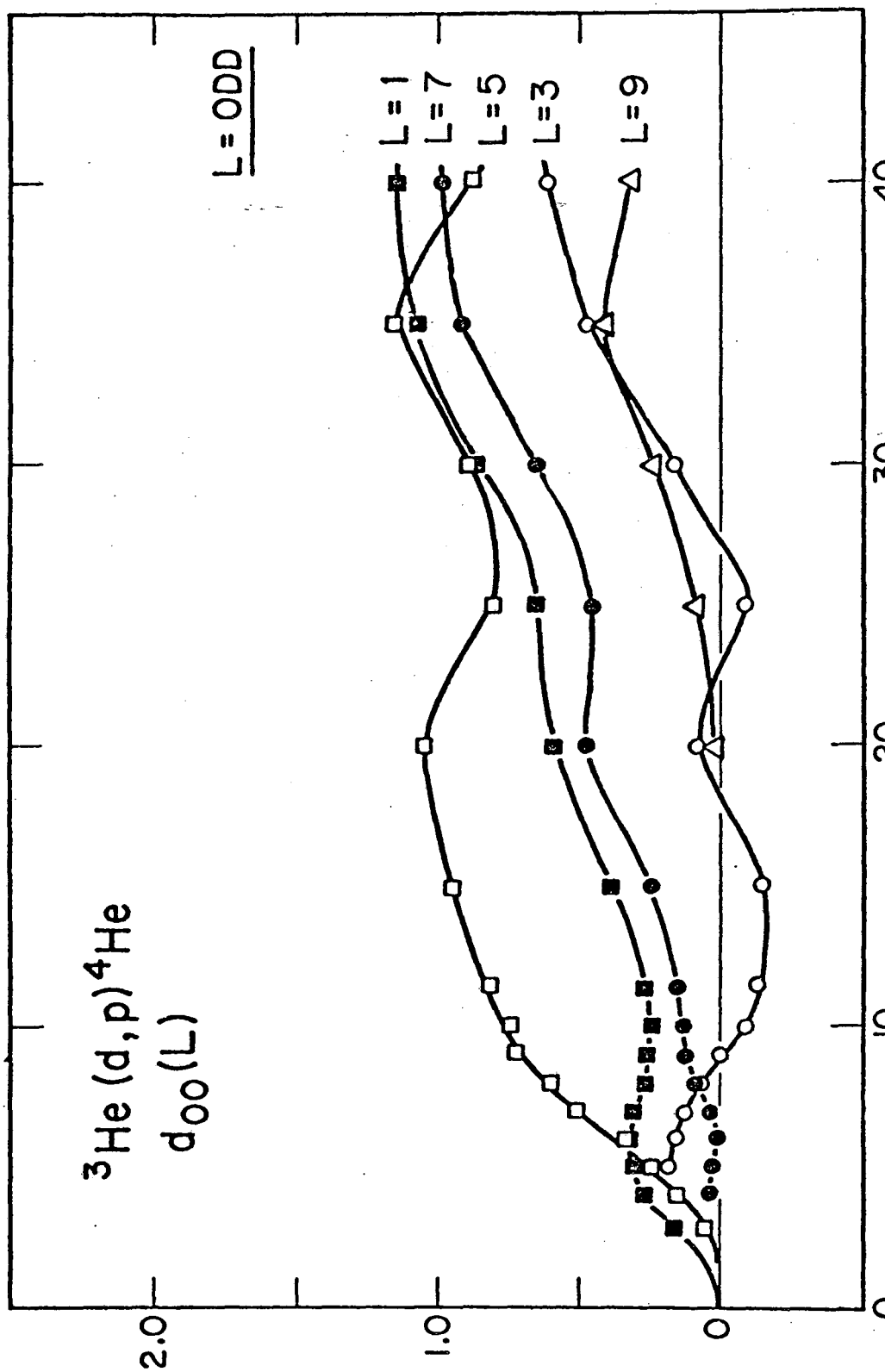

XBL756-3193

Fig. 9a

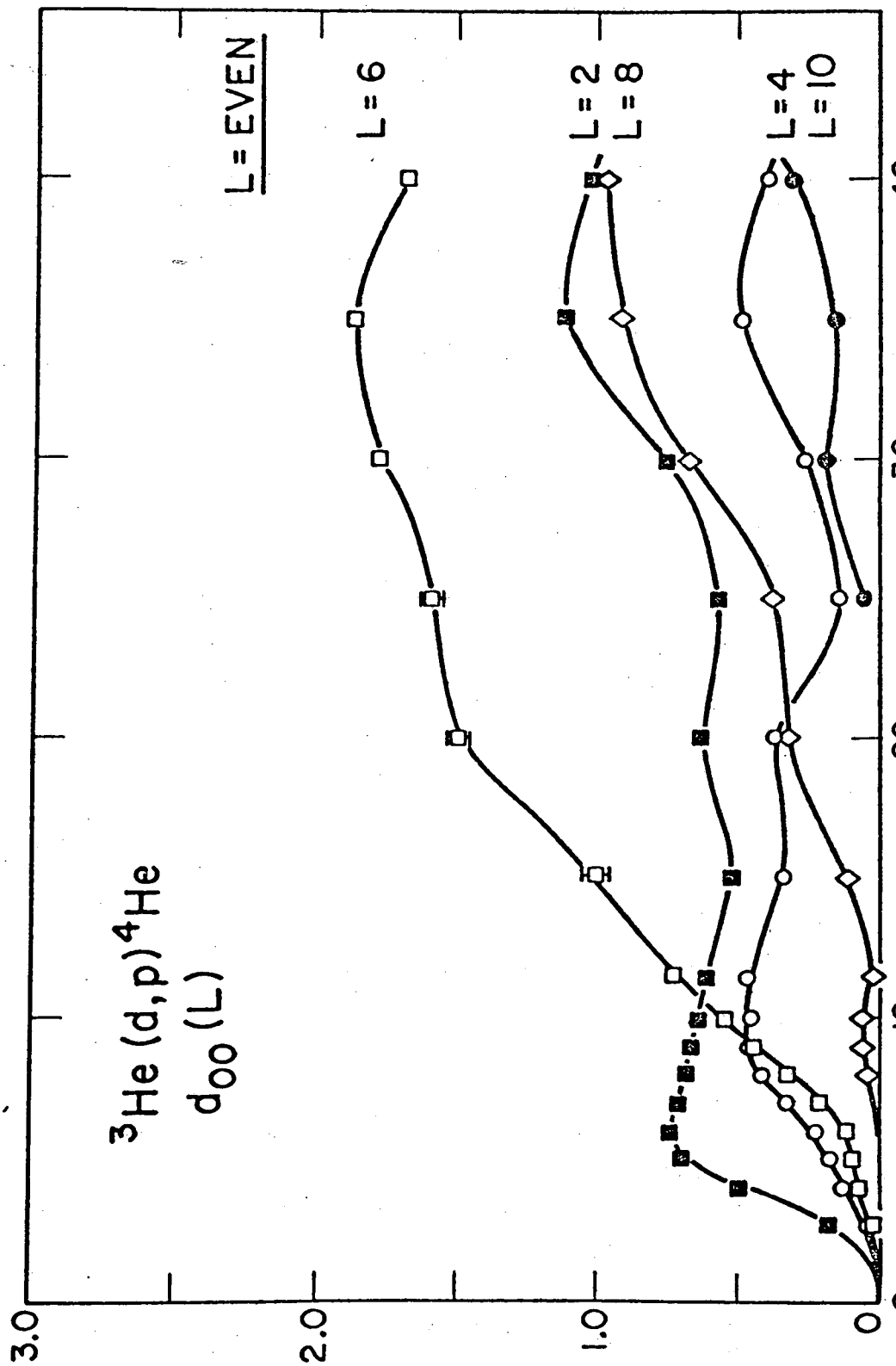

XBL756-3189

Fig. 9b

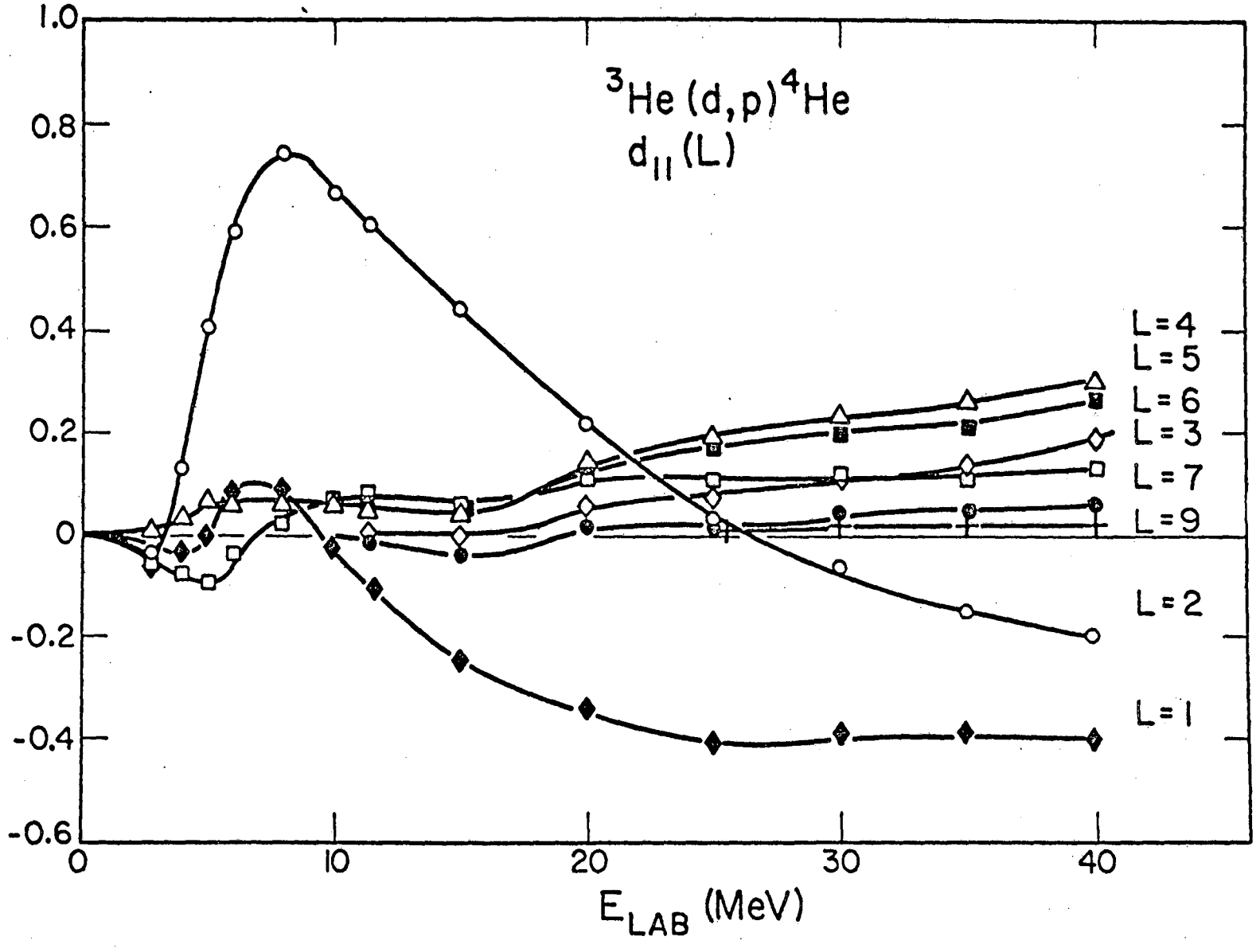

Fig. 10

XBL756-3194

LBL-14343

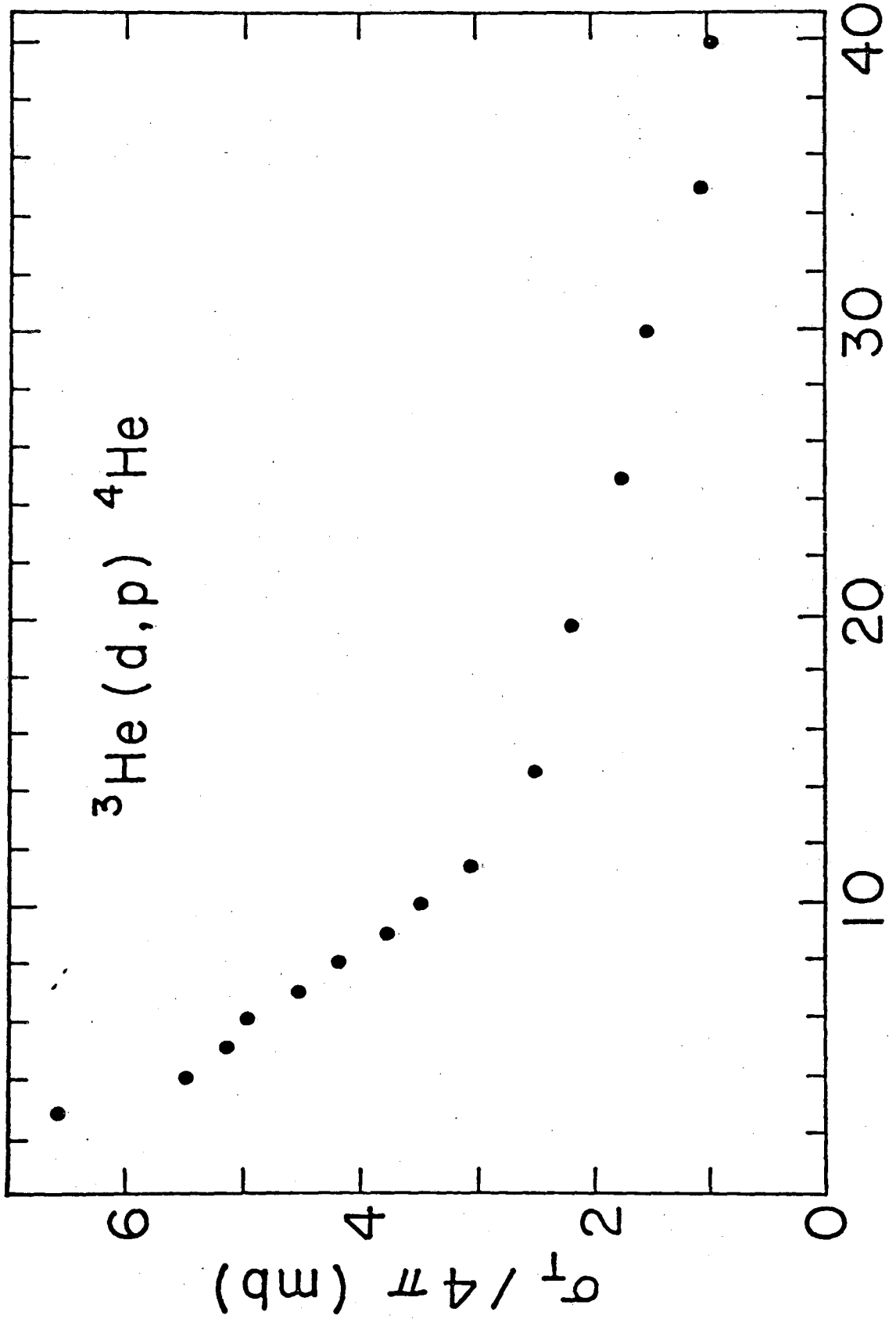

XBL761-2043

Fig. 11

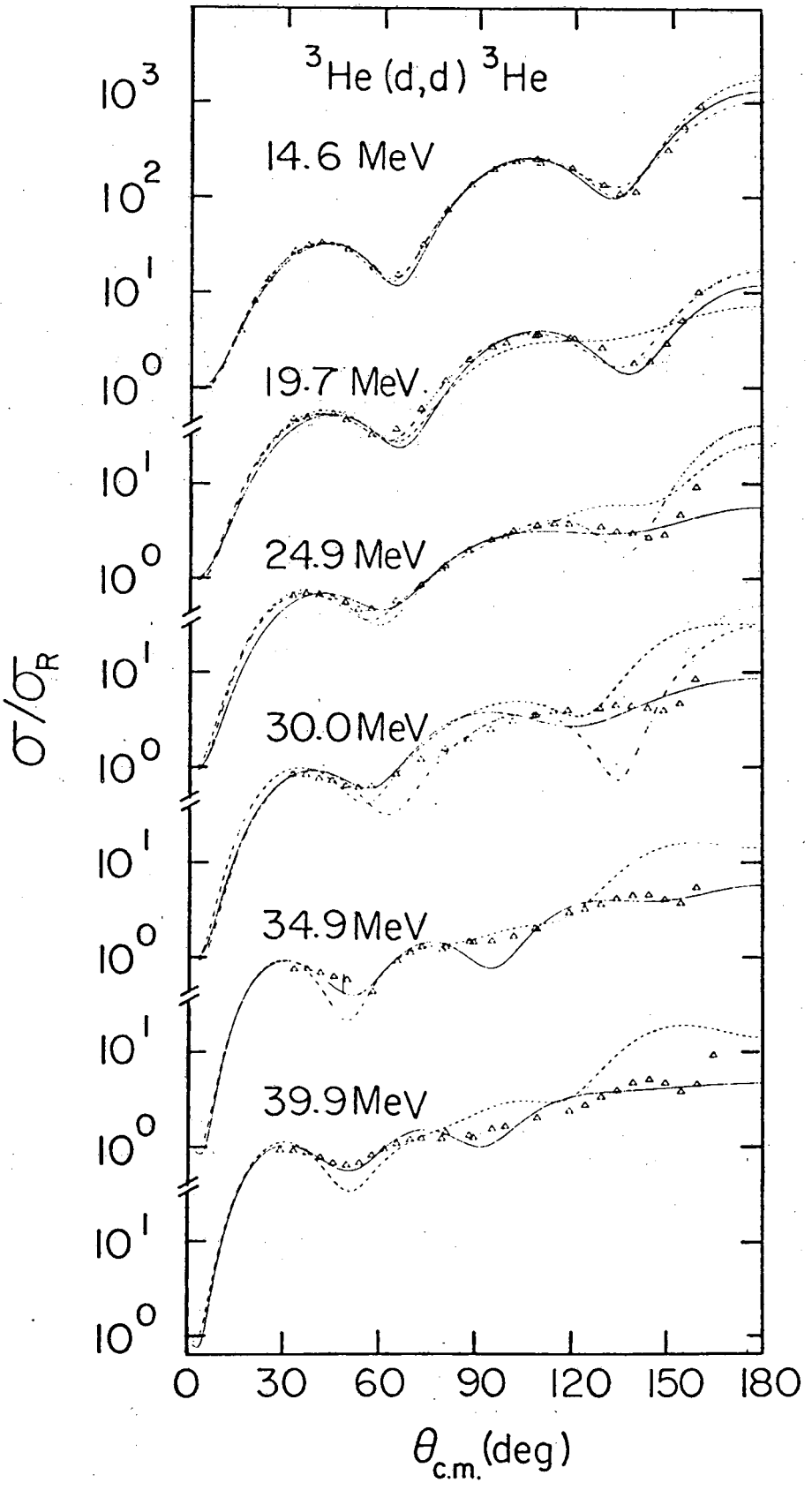
^{3}He (d,d) ^{3}He
14.6 MeV
19.7 MeV
24.9 MeV
30.0 MeV
34.9 MeV
39.9 MeV
σ/σ_R
10^3
10^2
10^1
10^0
0
30
60
90
120
150
180
$\theta_{c.m.}$ (deg)

Fig. 12

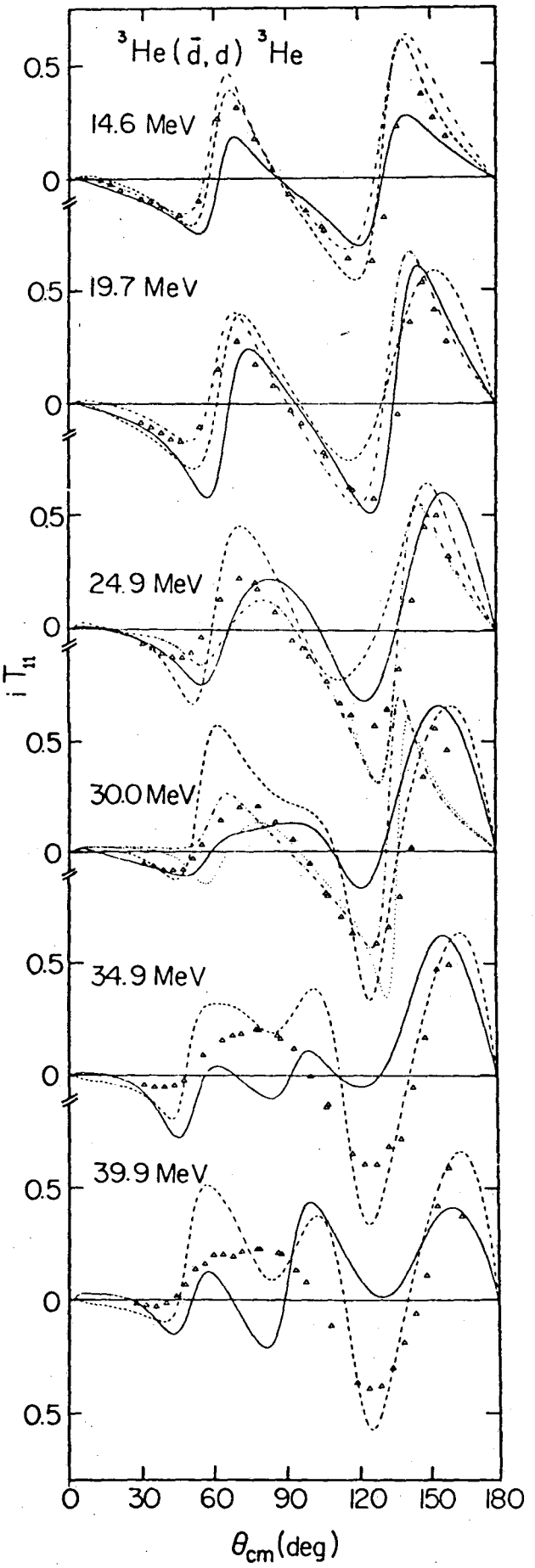
^{3}He($\vec{d}$, d) ^{3}He
14.6 MeV
19.7 MeV
24.9 MeV
30.0 MeV
34.9 MeV
39.9 MeV
0.5
0
iT_{11}
0
30
60
90
120
150
180
θ_{cm}(deg)

Fig. 13

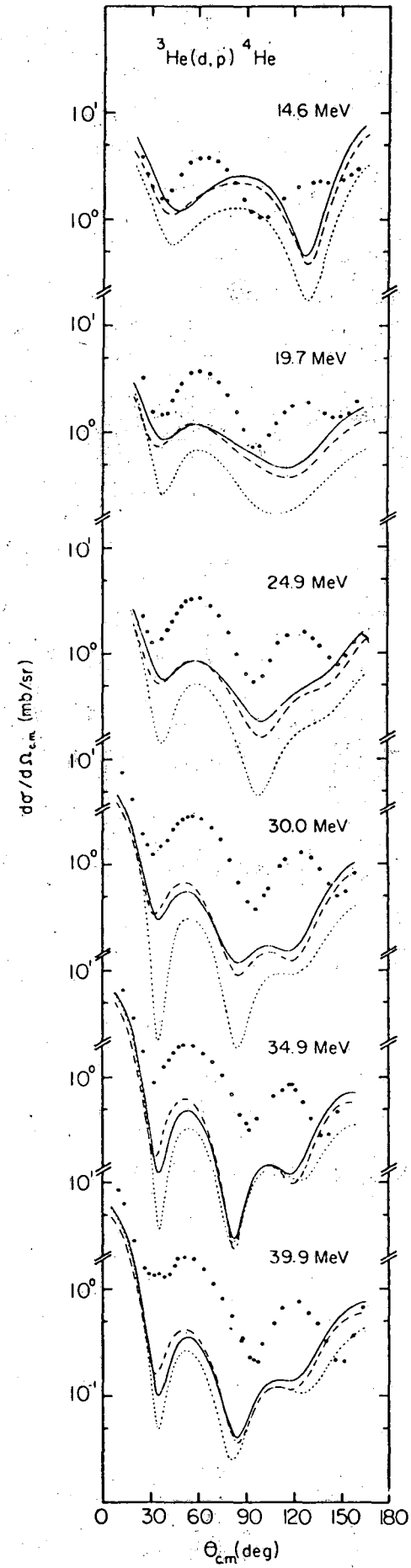
^{3}He(d,p) ^{4}He
14.6 MeV
19.7 MeV
24.9 MeV
30.0 MeV
34.9 MeV
39.9 MeV
10'
10°
10⁻¹
dσ/dΩ$_{c.m.}$ (mb/sr)
0 30 60 90 120 150 180
θ$_{cm}$(deg)

Fig. 14

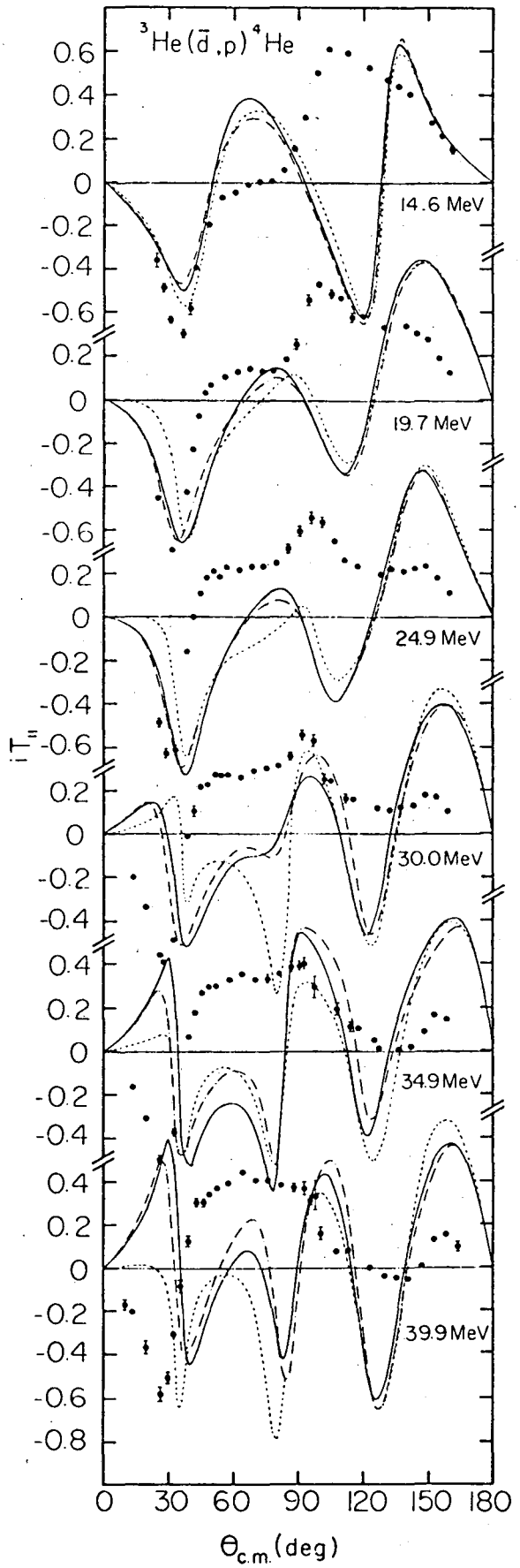
$^3He(\vec{d},p)^4He$
14.6 MeV
19.7 MeV
24.9 MeV
30.0 MeV
34.9 MeV
39.9 MeV
$iT_{=}$
$\theta_{c.m.}$ (deg)
0.6
0.4
0.2
0
-0.2
-0.4
-0.6
-0.8
0
30
60
90
120
150
180

Fig. 15

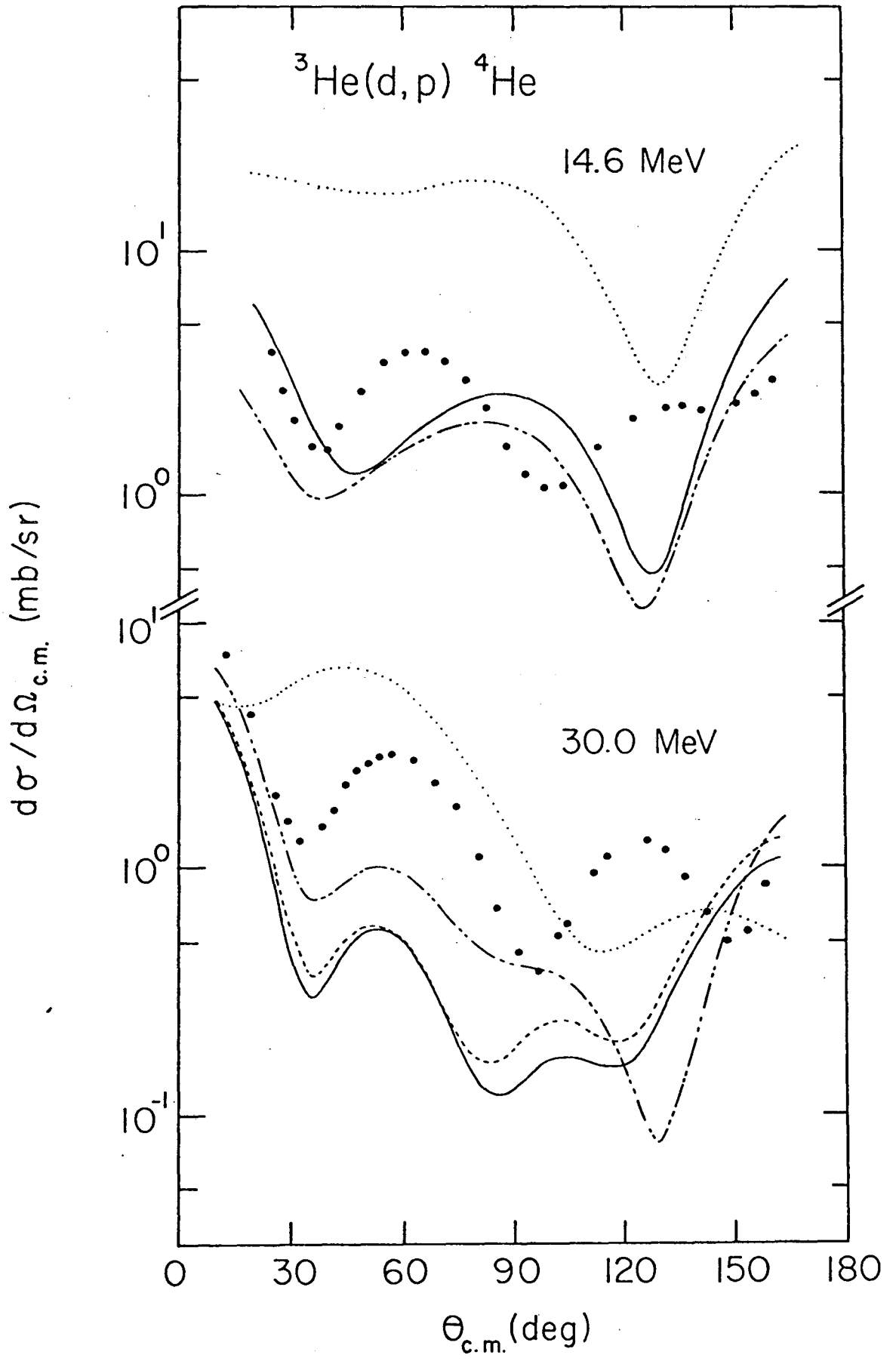
^{3}He(d, p) ^{4}He
14.6 MeV
30.0 MeV
10^1
10^0
10^{-1}
$d\sigma/d\Omega_{c.m.}$ (mb/sr)
0
30
60
90
120
150
180
$\theta_{c.m.}$ (deg)

Fig. 16

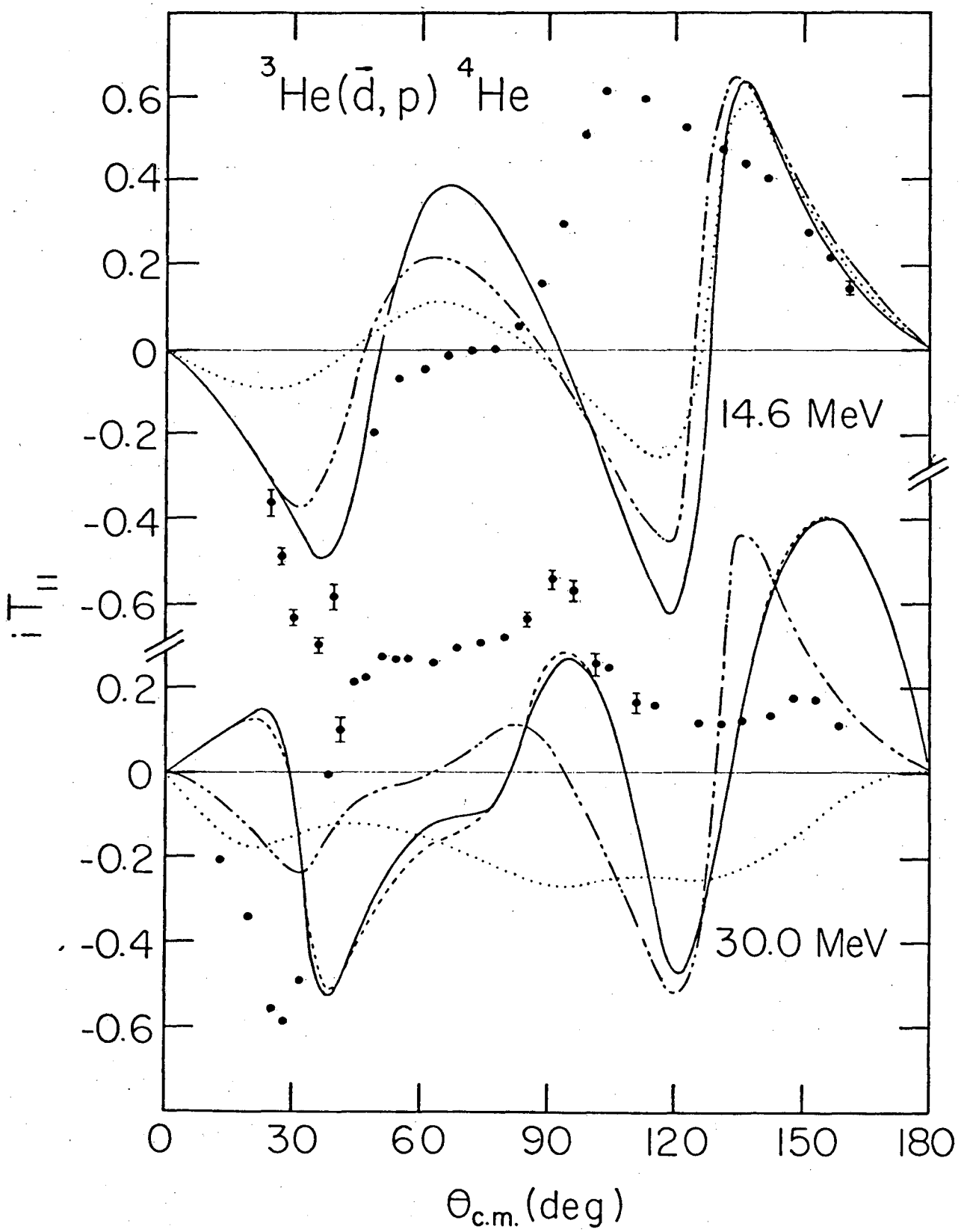
$^3He(\bar{d},p)\,^4He$
14.6 MeV
30.0 MeV
$T_{11}^{=}$
$\theta_{c.m.}$ (deg)
0.6
0.4
0.2
0
-0.2
-0.4
-0.6
0
30
60
90
120
150
180

Fig. 17

TECHNICAL INFORMATION DEPARTMENT
LAWRENCE BERKELEY LABORATORY
UNIVERSITY OF CALIFORNIA
BERKELEY, CALIFORNIA 94720